**Taking Nanotechnological Remediation Processes
from Lab Scale to End User Applications
for the Restoration of a Clean Environment**

Project Nr.: 309517
EU, 7th FP, NMP.2012.1.2

**WP3: Design, Improvement and Optimized Production of
Nanoparticles - Non-ZVI and Composite Nanoparticles**

DL 3.2 Assessment of Nanoparticle Performance for the Removal of Contaminants – Non-ZVI and Composite Nanoparticles

Katrin Mackenzie (UFZ), Anett Georgi (UFZ), Steffen Bleyl
(UFZ),Nimisha Joshi (UMAN), Beate Agnes Krok (UDE),
Christine Herrmann (USTUTT)

30 September 2016

List of co-authors:

Name, First Name	Partner Organisation	
Mackenzie, Katrin Georgi, Anett Bleyl, Steffen	Helmholz Centre for Environmental Research -UFZ	
Lloyd, Jonathan Joshi, Nimisha	University of Manchester	
Meckenstock, Rainer Krok, Beate-Agnes	Universität Duisburg-Essen	
Klaas, Norbert Herrmann, Christine	University of Stuttgart, VEGAS	

Reviewed by PAG member(s):

Name, First Name	Organisation	
Bruns, Johannes	Intrapore UG	
Matz, Pierre	Solvay Brussels	

Reviewed and agreed by PMG

Table of Contents

List of Figures

List of Tables

Glossary

Abbrevations and selection of symbols

(E)SEM	(environmental) scanning electron microscopy
AC	activated carbon
BET	estimation of specific surface area according to Brunauer-Emmet-Teller theory
Bnm	Bionanomagnetite
BTEX	benzene, toluene, ethylbenzene, xylenes
CMC	Carboxymethyl cellulose
COPR	chromite ore processing residue (from a site in Glasgow, UK)
DCA	dichloroethane
d_p	particle diameter
EDX	energy-dispersive X-ray spectroscopy
F.I.h	very hard standard water (US EPA, 2002)
F.I.m	moderately hard standard water (US EPA, 2002)
F.I.s	soft standard water (US EPA, 2002)
GC/TCD	gas chromatography with thermoconductivity detector
GW	groundwater
HA	humic acid
HCA	hexachloroethane
HPLC	high pressure liquid chromatography
IC	ion chromatography
ICP-OES	inductively coupled plasma - optical emission spectrometry
ISCO	*In-situ* chemical oxidation
k_{corr}	corrosion rate coefficient [e.g. h^{-1}]
K_d	sorption coefficient [e.g. $L \cdot kg^{-1}$]
k_{obs}	observed pseudo-first order reaction rate constant [e.g. h^{-1}]
M.I	Dorsilit® 8 sand
MPA	Materialpruefungsanstalt (material research laboratory)
MTBE; ETBE	methyl tert-butyl ether; ethyl tert-butyl ether
NPs	nanoparticles
nZVI	nano-scale zerovalent iron
PCBs	polychlorobiphenyls
PCE	perchlorethylene
PFOA/ PFOS	perflurooctanoic Acid / Pefluorooctanesulfonic Acid
PHAs	polycyclic aromatic hydrocarbons
PTFE	polytetrafluoroethylene
ROI	radius of influence
SLS/ DLS	static / dynamic light scattering
SQUID	superconducting quantum interference device
TCE	Trichloroethene
TeCA	tetrachloroethane
TEM	transmission electron microscopy
TOC	total organic carbon
UV-Vis/DRS	ultraviolet–visible spectroscopy/ diffuse reflectance spectroscopy
VC	vinyl chloride
WP	work package
XANES	X-ray absorption near edge spectroscopy
XRD	X-ray diffraction
XRF	X-ray fluoresence spectroscopy

1   Introduction

1.1   Background

NanoRem ("Taking Nanotechnological Remediation Processes from Lab Scale to End User Applications for the Restoration of a Clean Environment") is a research project, funded through the European Commission's Seventh Framework Programme.

The overarching aim of NanoRem is to support and develop the appropriate use of nanotechnology for contaminated land and brownfield remediation and management in Europe. NanoRem focuses on facilitating the practical, economic and exploitable nanotechnology for *in-situ* remediation. This can only be achieved in parallel with a comprehensive understanding of the environmental risk-benefit balance for the use of nanoparticles (NPs).

1.2   Introduction to DL 2.2 and DL 3.2

Workpackages WP2 and WP3 of NanoRem are dealing with design, improvement and optimized production of nanoparticles for *in-situ* remediation. WP2 is focused on zero-valent iron nanoparticles (nZVI) and WP3 on non-nZVI and composite particles. The final deliverables DL 2.2 (Assessment of Nanoparticle Performance for Removal of Contaminants – nZVI Particles) and DL 3.2 (Assessment of Nanoparticle Performance for Removal of Contaminants – Non-ZVI and Composite Particles) of the two WPs give an overview on the application areas and potential of the nanoparticles developed and aim to provide decision-making tools for problem owners and authorities. The two reports follow the same structure and should be seen as complementary. Table 1 provides an overview on the particle types presented in each of the two report deliverables. DL 2.2 and DL 3.2 mainly focus on the physical-chemical properties and reactivity of the nanoparticles. Particle transport, delivery and suspension stability are subject of DL 4.2 (Stability, Mobility, Delivery and Fate of optimized NPs under Field Relevant Conditions).

Table 1:   Overview on nanoparticle types presented in DL 2.2 and the present DL 3.2

DL 2.2 **Nanosized zero-valent iron**	DL 3.2 **Non-nZVI and composites**
NANOFER 25P	Nanoiron-oxide (Nano-Goethite)
NANOFER 25S	Carbo-Iron®
NANOFER STAR	Trap-Ox Fe-zeolites
FerMEG12 (A02, KKM02, nZVI-Labstar, KKM13)	(Palladized) Bionanomagnetite
Abrasive milling nZVI (NA56, NA64, NA74, NA84)	Non-ZVI metals (Mg/Al particles, Nano-FerAl)
	Barium Ferrate

2   Objectives of DL 3.2

With this report we want to close gaps in knowledge and open up new perspectives for the selection of remediation methods using particulate reagents and catalysts.

The practical use of nanoremediation has, up to now, been largely linked with the treatment of chlorinated solvents *in situ* and their selective transformation into less toxic, more biodegradable products. We want to summarize treatment approaches using nanoparticles and composites covering not only reduction but also oxidation and adsorption strategies. Figure 1 summarizes the particles studied and their principle mode of action which expands the toolbox for the design of nanoremediation operations. The spectrum of chemically treatable groundwater pollutants is extended from the conventional nanoiron-based options to non-halogenated substances and non-reducible metal ions. It covers reduction, oxidation and adsorption strategies.
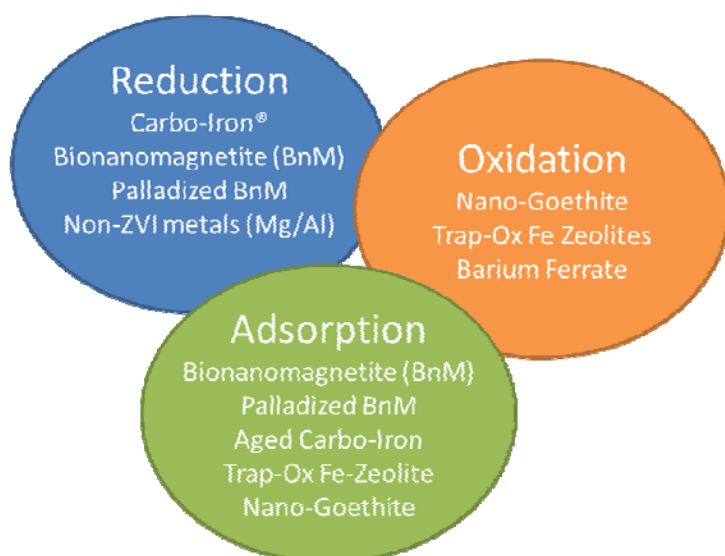
Figure 1:   Overview of WP3 particles allocated to three different reaction types

Thus, we seek to provide an overview of the studied non-nanoiron and composite particles, their physico-chemical properties and their anticipated application areas based on the knowledge of their principle mode of action and reactivity data gathered. This may support the aspired "step-change" in nanoremediation by adding new particle types with new target contaminants to the nanoremediation toolbox and by improving particle properties regarding suspension stability and subsurface mobility. Several WP3 particles even have the potential to add previously non-treatable contaminants to the portfolio of nanoremediation. Assuring the success of the nanoremediation concept requires proper selection of the particle type to be applied taking into account the target contaminant spectrum and remediation goals as well as specific site conditions. Most of the WP3 particles are newly developed or are employed in new uses.

Therefore, it is necessary to introduce the scientific community, possible end-users and the authorities to these new particle types and their basic behaviour. The particles are in various development states: from laboratory status to ready-for-market status, as will be elaborated within the chapters 6.1 to 6.7, which provides a detailed description of the individual particle types.

For a better overview, chapter 7 provides a tabulated easy-to-read summary of physico-chemical properties and reactivities followed by a tabular summary for providing a brief overview on treatable contaminants and general application areas of all non-NZVI particles and composite particles studied.

3   Overview of WP3 Nanoparticles

Within this report, the following particle types with their mode of action are described:

REDUCTION

– **Carbo-Iron®** contains metallic iron embedded in the grain of colloidal activated carbon (AC). As bare iron, Carbo-Iron® can reduce a broad range of halogenated hydrocarbons and is able to reduce/precipitate metals and metalloids. The close neighbourhood of the iron to AC extends the retention time at the reaction sites, which helps to prevent the generation of partial reduction products. The long-term support of microbial processes after its application in the field was observed. Carbo-Iron® particles are at the development state "*tested in the field and ready-for market".*

– **Bionanomagnetite and Palladized Bionanomagnetite** are biogenerated magnetic nanoparticles which show enhanced reduction properties. Bionanomagnetite is especially suited for adsorption of metals and metalloids. In addition, it shows magnetic properties and a high resistance to inhospitable aquifer conditions. Doping bionanomagnetite with Pd generates potent hydrogenation- and hydrodehalo¬genation catalysts. This opens up an extended target pollutant spectrum. Bionanomagnetite-based nanoparticles can easily be produced at larger scale and their development state is "*ready for field".*

– As **Non-ZVI metals** magnesium and aluminium particles **(Mg/Al particles)** were selected which show iron-like reaction potential but have a much lower material density which is identified as one of the crucial properties for subsurface transport. Within the project, both materials are intended to be tested for their principle reactivity and behaviour in sediment beds. Development to full application is not achievable within the given timeframe. The target pollutant chosen in NanoRem is PCE. The development state of the particles is "*lab-scale test".*

OXIDATION

– **Nano-Goethite** particles of the nano-goethite type are well-suited for stimulation of bioremediation of hydrocarbon-contaminated groundwater. By iron-reduction, oxidation of organic pollutants such as BTEX aromatics is accomplished. Nano-Goethite particles are at the development state "*tested in the field and ready-for market".*

– **Trap-Ox Fe-Zeolites** is a particle family tailored for *in-situ trapping and catalytic oxidation* of organic contaminants. Fe-zeolites are a powerful ISCO tool operating at near-neutral conditions and combine the high sorption ability for small organic pollutant (trap) with their efficient oxidation (ox). The catalytic generation of the strong oxidant OH-radicals from H_2O_2 for fast mineralization of recalcitrant pollutants such as fuel oxygenates, BTEX or even halogen-

ated substances, which are resistant to reduction processes (e.g. dichloroethane). Trap-Ox particles are at the development state *"ready for field".*

— **Barium Ferrate** is an example of a ferrate salt which exhibits low water solubility and thus could be used as a slow-release oxidant providing a depot effect in the sub-surface. The Fe(VI) ion is the active oxidizing species. The target pollutant chosen in NanoRem is toluene and the development state of the particles is "*lab-scale test".*

ADSORPTION

— The various types of **iron oxide nanoparticles** (Nano-Goethite and Bionanomagnetite) have a high affinity to metals and metalloids and can function as adsorbers. As the ability to bind the metals varies from metal to metal and oxide type to oxide type, the NanoRem iron oxides are tested for their adsorption potential towards several metal ions. Goethite is known to be especially suitable for AsO_3^{-3}, Ni(II), Zn(II), Cu(II). Nanomagnetite is able to adsorb (and reduce) Cr(VI) and bears a potential for adsorption of Pb(II), Cu(II), Zn(II) and Mn(II). All WP3 nanoiron oxides are regarded as *"ready for field".*

— **Aged Carbo-Iron®**: Carbo-Iron® is, even after its reaction phase, suitable to function as a strong adsorber for hydrophobic pollutants. Its use for the generation of sorption barriers for control of pollutants with high hydrophobicity (e.g. PCBs, PHAs…) is discussed.

— **Trap-Ox Fe-Zeolites** provide sorption properties for small organic substances (MTBE, BTEX, DCA and others) and can be exploited as sorption barrier. Regeneration of the adsorber can be carried out by activating the built-in catalytic function for targeted oxidation of enriched pollutants by addition of H_2O_2 (see above).

4 Methods for Particle Characterization and Reactivity Studies

Particle characterization techniques

A variety of methods was used in order to characterize physical-chemical properties, size and morphology of the particles developed within WP3. Microscopic imaging techniques like TEM or (E)SEM allowed identification of morphological structures and thus particle shape. Additionally, for characterization of particle size, or more precisely particle size distribution, various methods depending on particle size range and polydispersity were applied like dynamic light scattering (DLS), static light scattering (SLS), laser diffraction, EyeTech™ analysis (based on laser obscuration and dynamic image analysis) and Nanoparticle Tracking Analysis (NTA). With DLS methods additional parameters such as diffusion coefficients, hydrodynamic radii and surface potentials (zeta potential) can be estimated. The BET method as one routine technique for determination of the specific surface area allows characterization of the available surface for sorptive and reactive processes, which in particular is of importance for the estimation of surface-normalized reactivity parameter.

In order to characterize the chemical composition of the particles (element composition, oxidation state etc.), specific characterization techniques have been utilized or developed in the framework of NanoRem. These include methods such as ICP-OES (total iron) and spectrophotometric analyses (Fe^{2+}/ Fe^{3+} and total iron) after total digestion of particles, analysis of total organic carbon content

(TOC, for carbon containing particles, e.g. Carbo-Iron) and titrimetric methods (e.g. indirect Fe(VI) quantification in case of ferrates via chromite analysis with a standard ferrous ammonium sulfate solution (Licht et al., 2001)). In addition, UV-Vis/DRS for analysis of Fe speciation in Fe-zeolites, XRF (e.g. Si/Al ratio for zeolites), XRD, XANES (e.g. biomagnetite) as well as [57]Fe Mössbauer spectroscopy and SQUID magnetometry (both exclusively for iron-based materials) were applied. The zero-valent metal content was determined by indirect methods using acidification and subsequent analysis of hydrogen evolution (volumetric or by GC/TCD).

Reactivity studies

Since the particles described in this report employ various modes of contaminant removal (reduction, oxidation and immobilization) they differ in their target compounds and experimental setups for reactivity studies. Reactivity tests with particles for reduction processes (Carbo-Iron, Non-ZVI metals) followed the common protocols (for batch and column experiments) developed in NanoRem (DL4.1 Initial Particle Stability, Mobility and Delivery) using PCE as common model contaminant and further relevant target compounds. Organic hydrocarbons such as PCE and its degradation products (partially/completely dehalogenated hydrocarbons) were analysed by gas chromatography (mainly GC/MS). Formation of halogenide ions (e.g. Cl^{-}) was followed by ion chromatography.

In case of oxidative transformation (Nano-Goethite, Trap-Ox Fe-Zeolites, Barium Ferrate) contaminants of interest include non-halogenated hydrocarbons like BTEX (toluene as representative) or fuel oxygenates (e.g. MTBE for Fe-zeolites). Their degradation and intermediate product formation was analysed by GC or HPLC. TOC analysis was used to determine the degree of mineralization.

Batch and column experiments with reactive particles were evaluated in terms of pseudo-first order rate constants (k_{obs}), surface-area ore-mass-normalized reaction rate constants, mass recovery and particle efficiency. In addition, sorption isotherm data were obtained for particles with adsorption properties towards organic contaminants (Carbo-Iron, Trap-Ox Fe-zeolites).

The design of batch and column experiments depends on the specific particle type. Exemplarily, the setup for batch experiments using zero-valent metal as reagent according to NanoRem protocols is reported here. NANOFER 25S was agreed on as reference particle type. Experiments were performed in vials equipped with a gas-tight sealing (e.g., PTFE-lined septum or Mininert valve). Batch reactors were prepared under anoxic conditions, e.g. in an anaerobic chamber or by extensively purging with N_2 (or other inert gas such as Ar or He depending on analytical method applied) prior to adding the reagents to minimize oxidation of particles due to dissolved oxygen. Depending on the aim of the test (e.g. pH-dependence of reactivity, dependence on the constituents of the reaction medium or standard reactivity screening) a defined volume of NP suspension with a known concentration (or for non-NZVI particles also a defined mass of particles) was added to the N_2-purged anoxic fluid to achieve a target concentration. For standard reactivity screening typically a particle concentration of 1g/L active metal was used. An aliquot of contaminant solution is added to provide a desired initial contaminant concentration in water. For standard reactivity screening PCE was used typically in a concentration of c_{PCE} = 50 mg/L in order to simulate 1/3 of full solubility (source-relevant concentration). Temperature needs to be recorded in order to account for temperature corrections applying the Arrhenius function. The fluid used during the standard reactivity test is one of the standard type waters defined in NanoRem (F.I).

Additionally, soft standard type water was slightly buffered in order to exclude the pH-effect (drifting pH by metal particle's corrosion) on the reaction rate. Since bicarbonate comes closest to groundwater conditions, 2 mM $NaHCO_3$ (or 168 mg L^{-1}) was used for standard reactivity screening. Known liquid and/or gas volumes were sampled from the sealed vials using a syringe (gastight syringe for volatile chemicals). Prior to taking larger liquid sampling volumes (from 1 mL), negative pressure in the vial was precluded by inert gas injection. The retrieved/replaced sample volume (liquid/gas) has to be logged and considered in data processing. Sampling periods were adapted depending on the expected reaction rates from pre-experiments. Pressure and gas production were determined using an appropriate method (e.g. a digital pressure gauge or hydrogen content by TCD). Liquid samples were adequately handled according to the requirements of the analysis (e.g. filtered in order to remove remaining NPs (< 0.2 μm) prior to ion chromatography or extracted with organic solvents in presence of the particles for analysis of the target compounds, e.g., contaminants, or metabolites). PCE removal kinetics (by extraction) can be replaced by C_2-hydrocarbon development kinetics (gas analysis).

The reactivity of Nano-Goethite in biological degradation experiments is followed by the reduction of iron(III) to iron(II) and the simultaneous decrease of the contaminant concentration. Experiments were performed in batch or columns (with sediments from the remediation site). Samples (effluent) are taken frequently to measure the concentration of iron(III) and iron(II) by the ferrozine assay. The concentration of contaminant(s) is measured by GC/MS.

5   Application Areas and Potential based on Reactivity and Physical-chemical properties

5.1   Nano-Goethite

Responsible partner: UDE

Nano-Goethite is a material developed at the partner HMGU (now UDE). It consists of colloidal, nanosized iron oxide particles, coated with a layer of natural organic matter polymers. Its major application is bioremediation, where the iron oxides are readily available electron acceptors for microbial iron reduction (Bosch et al., 2010).

By applying a nanosized iron oxide which is in aqueous suspension, we can overcome transport limitations during injection. Bulk iron oxide sludges cannot be injected into soils because of their high viscosity, high affinity to sedimentation, and large particle size which will lead to immediate clogging. Our Nano-Goethite suspension shows a superior mobility in sediments (Tosco et al., 2012). At the same time, the reactivity for microbial iron reduction is greatly enhanced, as a low particle size causes high reactivity (Hochella et al., 2008).

5.1.1   Physical-chemical properties of Nano-Goethite

Due to the production process, the provided suspension of iron oxide NPs (100 g L^{-1}) additionally contained 5-6 g L^{-1} of TOC. The hydrodynamic radius of provided NPs was 240 ± 10 nm and was inde-

pendent from the suspension preparation procedure. A stability study showed that goethite NPs suspension is stable more than 24 h and revealed that the high TOC content provides sufficient stabilization of the NPs suspension envisioned for *in-situ* application. The measured zeta potential was -56 ± 2 mV indicating that electrostatic stabilization using organic matter polymers was provided.

A range of mobility experiments was performed at HMGU (later UDE), using reference porous media (Dorsilit® Nr.8 and field site material) according to the standardized experimental protocols (IDL4.1). These sediments were used in three different experimental set-ups: basic, simple flow-through column experiments, standardized columns, and cascading columns which mimic the radial decline of injection velocity. Determined transport parameters revealed a transport distance ($L_{T99.9}$) of 20.2 m for F.I.s, 12.9 m for F.I.m, and 21.8 m for F.I.h. For further details on suspension stability and transport properties of Nano-Goethite see DL4.2 (Stability, Mobility, Delivery and Fate of optimized NPs under Field Relevant Conditions).

Table 2:   Overview of physical-chemical properties and reactivity parameters of Nano-Goethite

Characteristics of Nano-Goethite	
Short description	Nanosized, colloidal goethite particles
Mode of action	Stimulation of microbial contaminant oxidation via microbial iron reduction
Chemical composition	FeOOH with organic coating
Average primary particle size ± RDS [nm] (specify: method applied)	220 ± 20 nm
Specific surface area [m^2/g]	140
Density [kg/m^3] (specify: true density, bulk density as powder, effective particle density with water-filled pores)	~ 3 (bulk powder)
Sedimentation rate [nm/min]	n.d.
Zeta potential [mV]	+30 (pH 7.1)
Type of stabilizers (in suspension)	humic acid
Content of stabilizers [%]	2
Zeta potential in presence of stabilizer [mV] (humic acid as stabilizer)	-45 mV (pH 8.2)
Reactivity data towards target toluene	k = 0.7 µM h^{-1} (with 4 g L^{-1} particles, $c_{toluene}$ = 1 mg L^{-1}, pH = 7; medium: UDE low salt groundwater)
Expected side-reactions	Generation of Fe^{2+}, generation of minor degradation metabolites like benzoic acid
Expected products after aging	Fe^{2+}, Magnetite

An overview of the physical-chemical properties and the reactivity parameters of nano-iron oxides is given in Table 2.

5.1.2   Reactivity of Nano-Goethite

The main application area for the iron oxide nanogoethite is the *in-situ* stimulation of bioremediation of hydrocarbon-contaminated groundwater. Up to now, the iron oxide nanogoethite is the only nanoparticle suspension for this application which:

- shows superior transport properties in the lab for a range of sediments and has been successfully injected at field sites

- has shown no renegade mobility after a first field injection

- has proven a high potential for the bioremediation of BTEX contaminations in the lab and in the field

- is available at industrial quantities and is largely non-toxic (see DL 5.2)

Nanogoethite NPs serve as reactive electron acceptors for microbial reduction and consequently stimulated microbial oxidation of pollutants such as BTEX compounds. The genus *Geobacter* is capable to use iron(III) as electron acceptor for the degradation of toluene.

Oxidation: $C_6H_5\text{-}CH_3 + 14\ H_2O \rightarrow 7\ CO_2 + 36\ e^- + 36\ H^+$ Eq. 1

Reduction: $Fe^{3+} + e^- \rightarrow Fe^{2+}$ Eq. 2
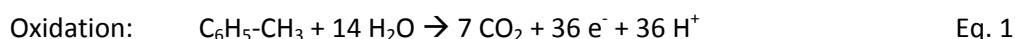
In the first step of anaerobic toluene degradation benzylsuccinate is formed due to the addition of fumarate to the methyl group of the toluene, catalyzed by the enzyme benzylsuccinate synthase. Afterwards succinyl-CoA and benzoyl-CoA (the main intermediate in the anaerobic degradation of aromatics) are formed due to a β-oxidation. Then, the aromatic ring is reduced and cleaved in a sequence of reactions to acetyl-CoA and CO_2. Benzoate is degraded to benzoyl-CoA compared to toluene by just one reaction step and therefore it is much more easily degraded by the autochthonous microorganisms (Fuchs et al., 2011).

One more potential application field for the UDE Nano-Goethite reaction arose during our R&D activities. Iron oxides are known to be highly adsorptive towards a range of heavy metals. So the idea came up to inject our iron oxide nanoparticles into heavy metal-contaminated groundwater aquifers, with the aim to establish an adsorptive (abiotic) barrier against further dislocation of the heavy metals. Initial laboratory studies indicated a superior adsorption capacity of our UDE Nano-Goethite towards As (Figure 2) and Cu. Further studies will help to understand the adsorption reactions, the long-term capacity and the sustainability of the adsorptive barrier against fluctuations of the surrounding biogeochemistry, and the feasibility under large-scale field conditions.
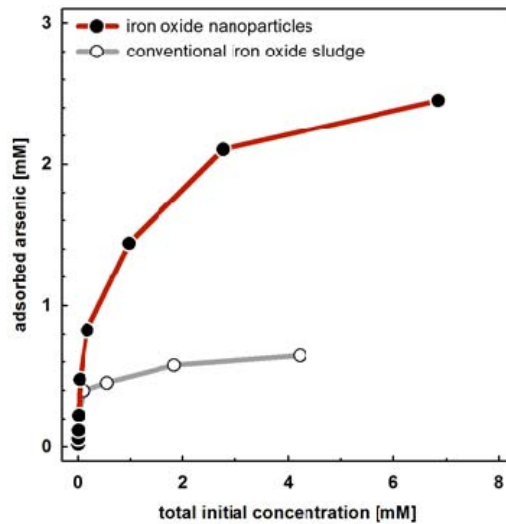
Figure 2:   Batch adsorption isotherm experiments. Arsenite was added to an iron oxide (nanosized colloids: red; bulk iron (goethite, Sigma, size > 1 µm: grey)) at pH 7 in a groundwater (low salt) medium and shaken overnight.

BTEX degradation results using sediment from a field site and two nano-iron oxides with coating and without are shown in Figure 3. Increasing Fe(II) content indicates iron-reducing microbial activity which leads to BTEX oxidation. In addition, enhancement of microbial iron reduction by humic acid coating compared to uncoated controls for the nanogoethite was found.
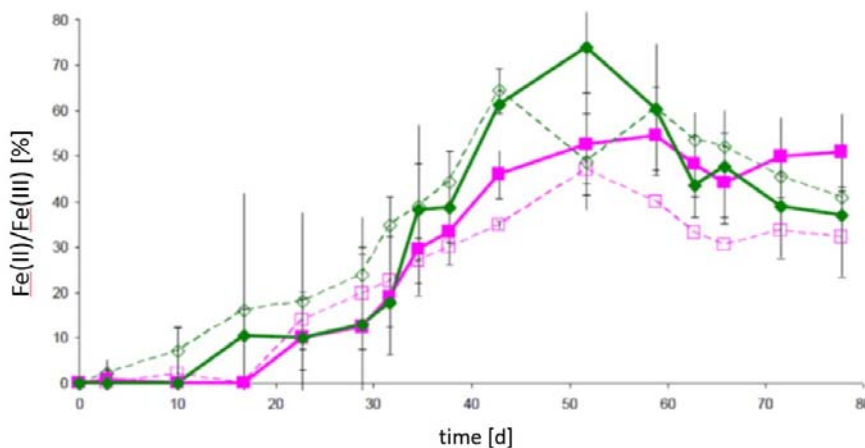
Figure 3:   Nano-Goethite amended with BTEX contaminated sediments and additional toluene (1 µM). Green: nano-ferrihydrite. Pink: nanogoethite. Open symbols: no coating. Closed symbols: humic acid coating. *Geobacter sulfurreducens* was added as an iron-reducing model microorganism. Initial iron oxide concentrations: 4 mM

Batch experiments with Spolchemie site sediments toluene and nanogoethite addition were performed to monitor the site-specific degradation, and to follow the enhancement of degradation due to our nanoremediation approach. Results showed no reaction in the negative controls, no significant change in Fe(II) and toluene in the incubations containing only site sediment and no nanoparticles, and a clear

increase in Fe(II) and decrease in toluene in the sediment incubations, which had been treated with Nano-Goethite (Figure 4).
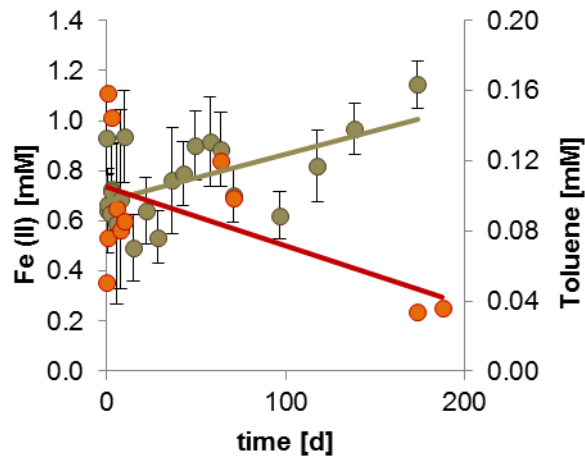
Figure 4: Batch incubation of Spolchemie II site sediment, groundwater medium, with the addition of 150 µM and 15 mM Fe(III) from UDE Nano-Goethite. Green: Fe(II), red: toluene. Results from positive, negative, and incubations without nanoparticles not shown. n = 3.
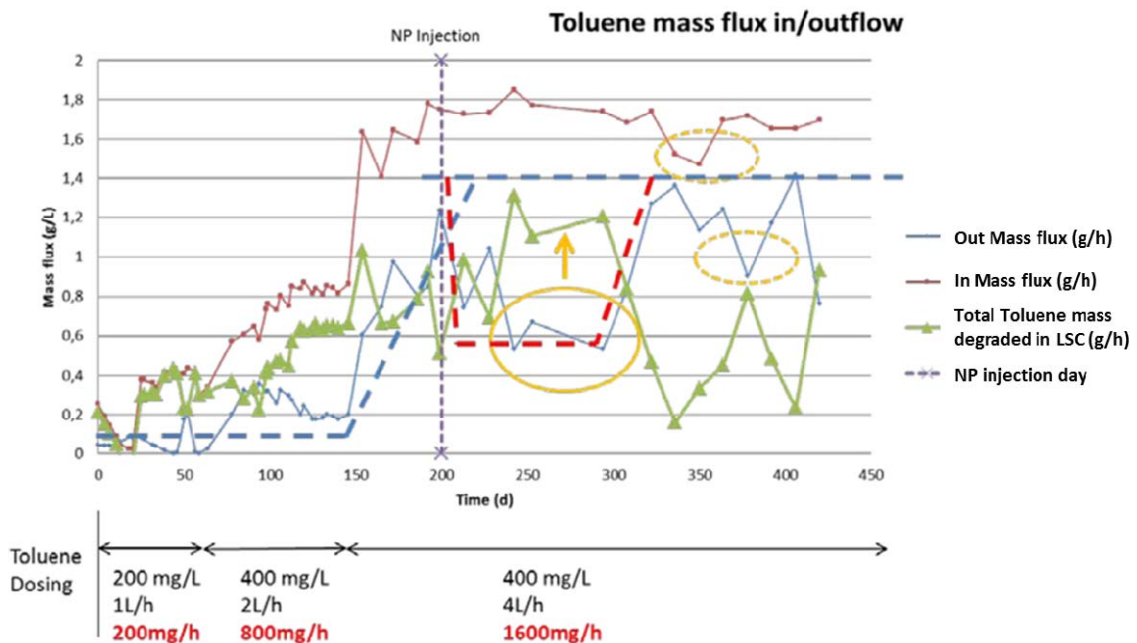
Figure 5: Outcomes of the VEGAS LSC container bioremediation experiment. The yellow full circle indicates a period of evident microbial degradation (stagnant mass flux and increase in toluene degradation), the yellow dotted circles indicate a decrease in flux.

The Nano-Goethite was successfully injected into the VEGAS LSC experiment and the radius of influence (ROI) was established as planned.

An increase in iron oxide-related bioremediation could be observed for about 100 days after injection (Figure 5). Based on the amount of toluene that was degraded, about 60% of the UDE nanogoethite was utilized. A certain share of the UDE nanogoethite is expected to not lie within the plume, as the vertical displacement during injection was higher than expected.

5.1.3   Influence of site conditions on particle applicability

A high ionic strength is influencing the stability of the particles leading to coagulation. Especially calcium ions are strongly influencing nanogoethite NPs leading to sedimentation, the critical coagulation concentration is 1.3 mM. This problem can easily be overcome by cation exchangers. The water at the field site used for the dilution of the concentrated Nano-Goethite solution prior to injection needs to be softened if the contained calcium concentration is higher than 1.3 mM. The Nano-Goethite NPs work best at neutral or slightly basic pH.

5.2   Carbo-Iron®

Responsible partner: UFZ

5.2.1   Physical-chemical properties of Carbo-Iron

Carbo-Iron® is a colloidal composite material developed at the partner UFZ. The composite contains metallic nano-iron structures with a mean cluster size about 50 nm which are generated within colloidal activated carbon (AC) particles (particle sizes < 1 µm). This leads to a composite reagent with unique properties suitable for the *in-situ* groundwater treatment. Carbo-Iron® has been designed based on existing knowledge of the nanoiron (nZVI) technology with the aim to generate particles with increased subsurface mobility and higher affinity to organic phases compared to the bare nZVI. To reach this the particles were designed to provide higher suspension stability, avoid high agglomeration tendency, allow subsurface particle transport and provide the ability for source targeting (Mackenzie et al. 2012).

By embedding the nano-sized iron reagent deep into the AC, the iron-inherent high agglomeration tendency (due to magnetic attraction forces) is counteracted. The iron is "trapped" in the AC particles which functions as spacers between the iron structures. During the particle design process parameters such as particle size, particle density and surface charge were adjusted to obtain optimal particle transport properties. With a Fe(0) content of 20 to 30 wt%, the porous composite has an effective density in water of ≈2.1 g cm^{-3} (water-filled pore volume) which comes close to natural colloids. Suspension stability and colloid mobility in the subsurface are influenced by the particle size, which is a crucial parameter for an injectable *in-situ* reagent.
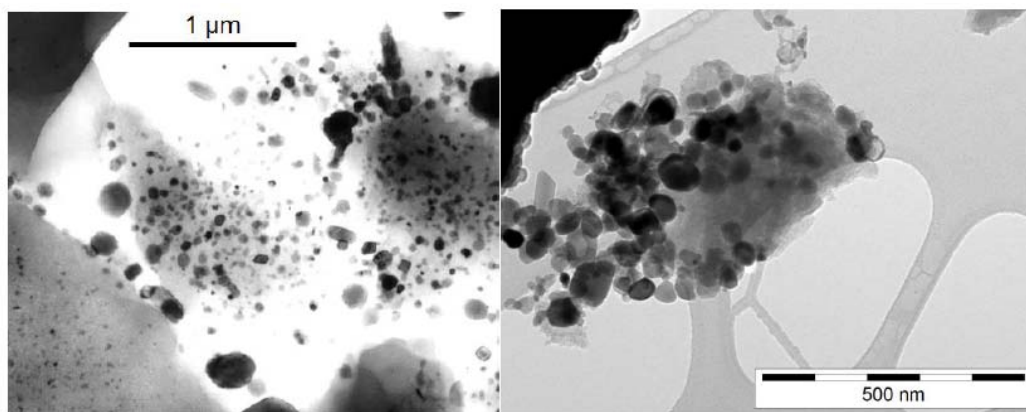
Figure 6:   Bright field TEM image of two Carbo-Iron® batch samples (thin slices) showing iron struc-
tures having a mean cluster size of less than 100 nm (left image taken at Leipzig Universi-
ty, right image taken by UPOL).

Based on the density of the composite, one can estimate the optimal particle size for subsurface
transport being in the range of 0.5 to 2 µm (Elimelech et al. 1995, Ryan and Elimelech 1996). This size
range has therefore been chosen for the AC colloid precursor which determines the final particle size
of the Carbo-Iron. This means, even though the embedded reactive metallic iron is nano-sized, the
particle itself is not. The colloidal carrier AC has been produced by milling of commercial AC powder
(particle size of Carbo-Iron® used in NanoRem is d_{50} = 0.8 to 1.4 µm). The synthesis is based on wet
impregnation of the AC with iron salts and carbothermal reduction under inert gas atmosphere (Bleyl
et al. 2012). An air-stable product is synthesized which can be easily stored as dry powder without
losing metallic iron and thus its reactivity in water. Figure 6 shows the composition of Carbo-Iron® in
TEM images. Thin slices of the material embedded in resin (left) show that the majority of the iron is
located within the carbon grain.

Table 3:   Overview of physical-chemical properties and reactivity parameters of Carbo-Iron

Characteristics of Carbo-Iron	
Short description	Embedded Fe(0) in microscale activated carbon (AC) to form an AC/Fe composite
Mode of action	Chemical reduction at Fe(0) combined by hydro-phobic sorption at AC (trap & treat)
Chemical composition	Fe_{total} = 35 [%] Fe (0) = 25 [%] Fe_3O_4 = 14 [%] O = 6 [%] C_{total} = 45 [%]
Average primary particles size ± RDS [nm] (laser diffraction)	d_{10} = 500 [nm] d_{50} = 1100 [nm] d_{90} = 2500 [nm]

Specific surface area [m^2/g]	600 - 700
Density [kg/m^3] (specify: true density, bulk density as powder, effective particle density with water-filled pores)	0.6 (bulk density); 2.1 (effective particle density)
Sedimentation rate [nm/min]	n.a.
Surface charge [mV]	n.a.
pH of suspension	7…9
Reactivity data towards target PCE	$k_{obs} = 6.3 \cdot 10^{-3}$ h^{-1} (with 1 g/L Fe(0), $c_{PCE} = 50$ mg L^{-1}, pH = 7.8; medium: F.I.m) $k_{SA} = 4.1 \cdot 10^{-4}$ L/(h m^2) (surface area estimated from TEM data, assuming spherical iron species and tight Fe size distribution)
Sorption data towards target PCE	log K_D = 4.1
Corrosion data	$k_{corr} = 2.3 \cdot 10^{-3}$ h^{-1} (with 1 g/L Fe(0), $c_{PCE} = 50$ mg L^{-1}, pH = 7.8; medium: F.I.m)
Expected side-reactions	Hydrogen evolution, decrease redox potential, pH increase
Type of stabilizers (in suspension)	Carboxymethyl cellulose, humic acid
Content of stabilizers [%]	5…20 wt% CMC (referred to $m_{Carbo-Iron}$) depending on scope of application
Duration of suspension stability [days]	1 to several days (depending on $c_{stabilizer}/c_{particle}$)
Zeta potential in presence of stabilizer [mV]	-23 (pH = 7; 1mM KNO_3; $c_{particle}$ 1 g L^{-1} with 20 wt% CMC)
Expected products after aging	Iron oxides on activated carbon

5.2.2   Reactivity, colloid stabilityt and sorption to Carbo-Iron

As described above Carbo-Iron's inherent properties can be denoted to both activated carbon (AC) and the electron rich structures of zero-valent iron within the AC, which make Carbo-Iron® a trap-and-treat reagent. Adsorptive enrichment of halogenated organic contaminants (HOC) onto Carbo-Iron's AC backbone and near the Fe centres facilitates their effective degradation (Figure 7) (Mackenzie et al. 2016).
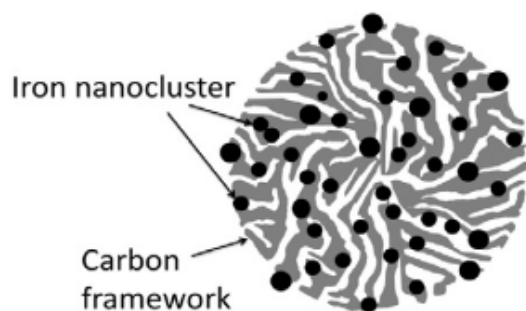
Figure 7:   Schematic illustration of composite material Carbo-Iron

The reactive component iron is consumed during application mainly by two overall processes: dechlorination as the target reaction (according to Eq. 3 for PCE with n = 3…5) and the iron corrosion.

$$n\,Fe^0 + C_2Cl_4 + (2n-4)\,H_2O \xrightarrow{k_{obs}} n\,Fe^{2+} + C_2H_{(2n-4)} + (2n-4)\,OH^- + 4\,Cl^-$$ Eq. 1
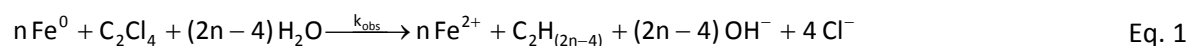
As shown in degradation experiments, Carbo-Iron® is able to effectively reduce chlorinated hydrocarbons such as PCE to non-chlorinated substances. Typical reactivity parameters for PCE as target contaminant are compiled in Table 3. With this, the material can be utilized to drastically reduce risks posed by chlorinated water substances.

Corrosion processes (anaerobic corrosion in absences (Eq. 4) and aerobic corrosion in the presence of dissolved oxygen) decrease the proportion of iron which is available as reducing agent in contaminant dechlorination. However, corrosion of nZVI is an unavoidable process in water. In order to efficiently utilize the iron, suppression of the corrosion processes is a continuing goal (further discussed in 6.2.3.).

$$Fe^0 + H_2O \longrightarrow Fe^{2+}\,OH^- + H_2$$ Eq. 2

Depending on the sorption affinity, a broad variety of possible contaminants are found to be efficiently treatable by the composite Carbo-Iron. Exemplarily, PCE represents a model contaminant, which has a high sorption affinity to AC due to its hydrophobic nature. Degradation of model compounds such as PCE has been investigated in several test media for evaluation of kinetic data in the harmonized protocol summarized in DL 4.1 (Initial particle stability, mobility and delivery).

Reactivity in typical groundwater samples from different field sites

The comparison of PCE degradation and product formation (Cl-free C2-hydrocarbons) in different test media (site groundwater, standard type water etc.) show no significant difference (Figure 8). Even the addition of the colloid stabilizer CMC, which will be present while Carbo-Iron® is injected into the contaminated aquifer, has no adverse effect on contaminant removal which is a crucial prerequisite for implementation of the Carbo-Iron® technology. In the first pilot-scale field tests the use of Carbo-Iron® was successfully demonstrated. Extended longevity of the Carbo-Iron® action within the treatment zone showed evidence of microbial activity (Mackenzie et al. 2016).
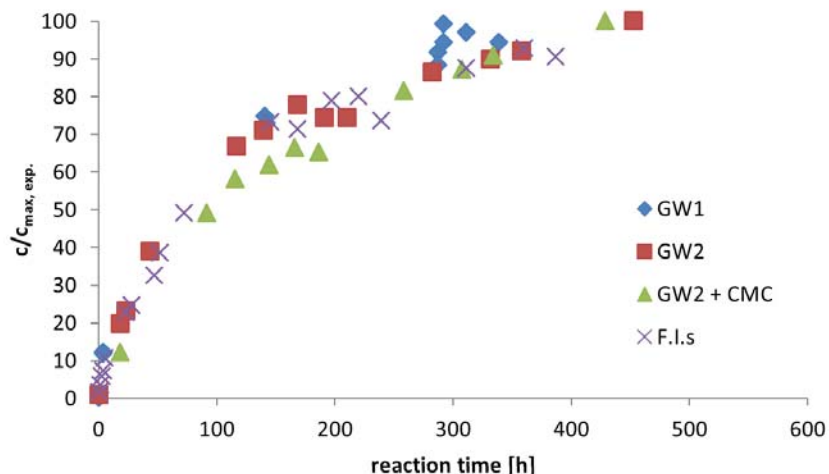
Figure 8: C_2-hydrocarbon formation kinetic as c/c_{max} for the degradation of the model compound PCE in various reaction media with suspended Carbo-Iron® colloids ($c_{0,PCE}$ = 50 ppm, GW1, GW2: groundwater from different field sites; GW2 + CMC: groundwater with the additive CMC and soft standard type water F.I.s; $c_{particle}$ = 5 g L^{-1} ($x_{Fe(0)}$ = 21 wt%); c_{CMC} = 1.25 g L^{-1}; pH= 8.3 (GW1); pH = 8.7 (GW2); pH = 7.4 (F.I.s)).

General application mode for Carbo-Iron® colloids

- Reductive dehalogenation of halogenated hydrocarbons (e.g. chloroethenes, highly chlorinated alkanes, bromohydrocarbons)
- Sorption of hydrophobic compounds (and prolonged retardation within treatment zone)
- Sorption and reductive immobilisation of dissolved metals and metalloids
- Microbial assisted self-cleaning (ENA after Carbo-Iron® action due to hydrogengenerated, Fe-oxides available for iron-reducing bacteria, AC as porous material for microbial colonization)
- Sorption-assisted hydrolysis

Selection of treatable substances:

Halogenated hydrocarbons:

- chlorinated ethenes (PCE, TCE, DCE, VC)
- chlorinated methanes (CCl_4, $CHCl_3$)
- chlorinated ethanes (hexachloroethane, TeCA…)
- brominated aliphatics (1,2-Dibromoethane, Vinylbromide)
- polychlorinated aromatics and biphenyls (presumably)

Inorganics:

- inorganic anions: nitrate, perchlorate
- metal ions and metalloids: e.g. As^V, Cr^{VI}, Pb^{II}

The highest application potential is seen in sorption-assisted reductive dehalogenation and in the reduction/immobilization of metal irons and metalloids (e.g. NO_3^-, Cr^{VI+}, As) as illustrated in Figure 9:
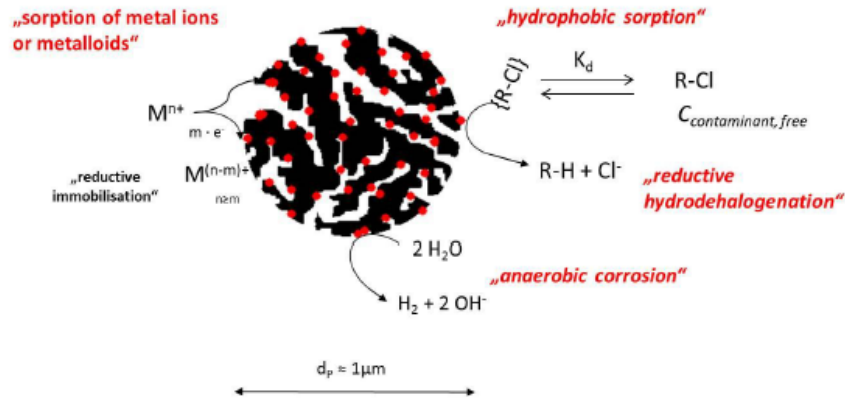
Figure 9:   Transformation pathways of potential contaminant types at Carbo-Iron

Colloid stability

The stability of particles suspensions is one of the parameters to evaluate and compare different particle types regarding their applicability as injectable reactive colloids for *in-situ* treatment. Particle suspensions should be stable for several hours in order to avoid clogging effects during field injection. In order to avoid fast agglomeration, which would lead to high sedimentation rates and thus instable suspensions, additives such as polyanionic colloid stabilizers are usually applied to stabilize nZVI suspensions (Lin et al., 2010; Phenrat et al., 2011; Phenrat et al., 2008). Carbo-Iron's suspension stability is already enhanced compared to nZVI suspensions, the addition of polyanionic stabilizers, such as CMC or humic acid (HA), further helps to enhance suspension stability. Here, CMC as colloid stabilizer is discussed. Sedimentation experiments with varying CMC concentrations (1 to 25 wt% referred to particle mass) were carried out in order to find the optimal suspension formulation.
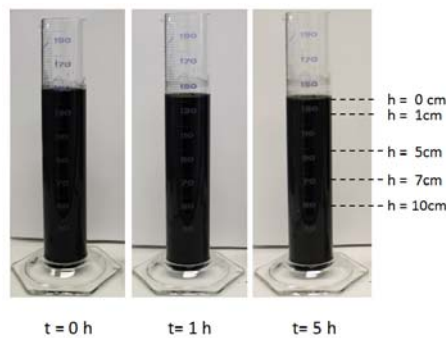
Figure 10: Sedimentation tests of stabilized Carbo-Iron® suspensions ($c_{particle}$ = 1 g/L; $c_{electrolyte}$= 10 mM NaCl; pH = 6.5, V_{sample}= 0.5 mL at different sampling heights h cm below water table)

Addition of ≥ 15 wt% CMC to Carbo-Iron® suspensions ($c_{CMC} ≥ 0.15 \cdot c_{Carbo-Iron}$) forms stable suspensions in a broad concentration range $c_{particle}$= 1 to 20 g L^{-1} (Figure 10). CMC concentrations below 5 wt% ($c_{CMC} ≤ 0.05 \cdot c_{Carbo-Iron}$) stabilize only insufficiently. Figure 11 shows the remaining particle fraction in suspension at a pre-defined level below the water table shown as a function of sedimentation time (h = 1 cm which is only slightly affected by the "particle curtain" falling from regions above).
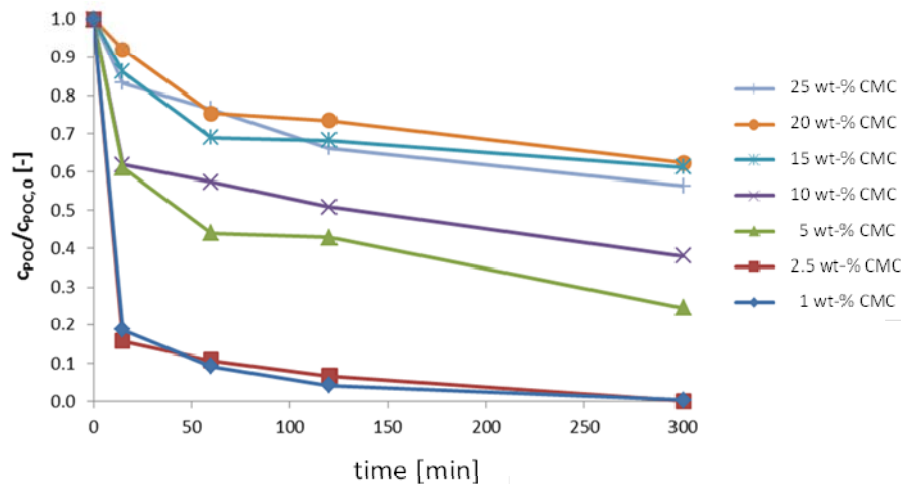
Figure 11: Influence of CMC on Carbo-Iron® suspension stability ($c_{particle}$ = 1 g/L; $c_{electrolyte}$ = 10 mM NaCl; pH = 6.5, V_{sample} = 0.5 mL taken at h = 1 cm below water table; c_{CMC} referred to particle mass $m_{CMC} \cdot 100/m_{particle}$ in wt%).

Fast sedimentation of an oversize fraction is observed in all suspensions, which can be seen by the initial fast decrease in the relative particle concentrations (c/c_0; t < 0.5 h). This fraction is small (< 15 %) at high CMC concentration but becomes more dominant with decreasing CMC content due to an entraining effect. Figure 10 shows that Carbo-Iron® is well dispersible and can be kept in suspension for a considerable time. Since injectability, suspension stability and a certain subsurface mobility are major preconditions for a successful application as particulate *in-situ* agent, the check for the principle applicability needs to be carried out by sedimentation and mobility studies.

5.2.3   Influence of site conditions

The application potential of Carbo-Iron® colloids strongly depends on the conditions in natural environments and the particle specific properties. Therefore aerobic media should strictly be avoided in order to prevent fast oxidation of the metallic species. Typical pH values for groundwater are in the range of 5.5 to 8 and are considered within the Carbo-Iron operation window. In strong acidic media, Carbo-Iron should not be applied because of fast iron loss. Furthermore, permeable aquifers ensure optimal particle delivery to the contaminated zone. Experiences gained at field scale outside Nano-Rem reveal that Carboxymethyl cellulose (CMC) needs to be well soluble in water and should not have a major impact on the water viscosity.[1] We recommend a molecular weight M_{CMC} < 100 kDa. With the product Walocel CRT 30G (DOW Cellulosics) good results in relation to both suspension stability in typical groundwater and migration of colloid suspensions in natural porous media were received. Depending on the contaminant distribution at a certain field site different application

---

[1] Carboxymethylcellulose with the formula [$C_6H_7O_2(OH)_x(OCH2COONa)_y$]$_n$ should be well water soluble when the substitution degree y is in the range of 0.6 to 0.95. For the Walocel CRT 30G, a substitution degree of 0.8 to 0.95 is given and a molecular mass of <10 kDa

modes concerning injection and particle transport are conceivable: *a*) source zone mode, whereas reactive particles should be immobilized in a confined contaminated area *b*) plume mode, which means a broad reactive zone should be implemented if faced with low concentrations of dissolved pollutants. Both scenarios can be addressed using tailored suspension recipes in order to adjust the suspension stability and particle transport with targeted deposition on sediment grains. CMC-stabilized Carbo-Iron® suspensions up to 30 g L^{-1} (~ 7.5 g L^{-1} Fe^0) are injectable, which allows achieving final sediment loadings of about 1 wt% and simultaneously prevent clogging of flow paths. Results from column tests with stable Carbo-Iron® suspensions in field site material and groundwater from the field site expose an inhomogeneous distribution in the direction of the groundwater flow. Even on microscale level a non-uniform particle deposition pattern is obviously a result of preferred deposition sites at grain surfaces (Figure 12).
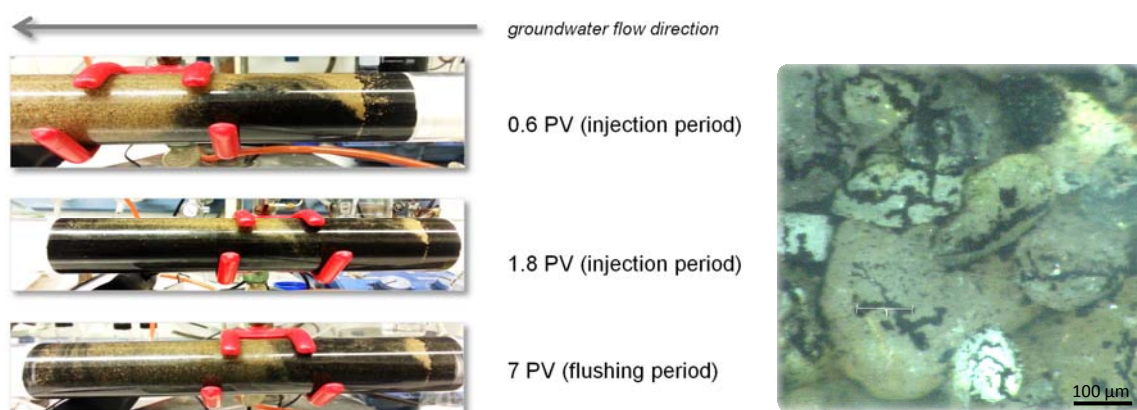
Figure 12: *Left* – Migration of Carbo-Iron® colloids ($c_{particle}$ = 15 g L^{-1}, c_{CMC} = 1.5 g L^{-1}) performed in field site groundwater (v_{eff} = 10 m d^{-1}, pH 8.1; alkalinity 250 mg CaCO$_3$ L^{-1}, electric conductivity 1306 µS, total water hardness 680 mg CaCO$_3$ L^{-1}) and porous media from the Hungarian site (Balassagyarmat, sieve fraction of sediment d$_s$ < 2 mm); *Right* – deposition pattern for injected Carbo-Iron® colloids ($x_{Fe(0)}$ = 21 w.t%, d_{50} = 1.3 µm) on grain surface after removal of mobile particle fraction with simulated groundwater flow (v_{eff} = 0.25 m d^{-1}) – magnification: 175x.

5.3   Trap-Ox Fe-zeolites

Responsible partner: UFZ

Trap-Ox Fe-zeolites is a particle family tailored for *in-situ trapping* of organic contaminants by adsorption and catalytic *oxidation* in combination with oxidants such a hydrogen peroxide. Zeolites can be synthetized at large scale in various modifications differing in channel structures and Si/Al ratio. The optimal choice of Trap-Ox Fe-zeolites depends on the type of contaminants and conditions at the field site. Within NanoRem, optimized injectable suspensions were developed for two zeolite types: **Trap-Ox Fe-BEA35 and Trap-Ox Fe-MFI120**. Their field of application is *in-situ* trap&treat of a variety of typical groundwater contaminants such as MTBE, ETBE, chlorinated ethanes and ethenes and BTEX. Trap-Ox Fe-BEA35 is available in large quantity for field testing. In addition, a fluorescence labelling approach was developed for particle tracking (Gillies et al. 2016).

5.3.1   Physical-chemical properties of Trap-Ox Fe-zeolites

Trap-Ox Fe-zeolites are microporous alumosilicates which are loaded with iron ions by ion exchange and subsequent stabilization methods. Due to their high specific surface area and well-defined narrow pores they act as adsorbents for small organic molecules.

According to SEM analyses the two Trap-Ox particle types have a spherical shape with small primary particles (200 to 400 nm) and their particle size in aqueous suspension is about 500 nm, determined by DLS measurements. Similar to silica surfaces, the Fe-zeolite surface bears a net negative charge over a wide pH range (pH ≥ 3, see DL 4.2 Stability, Mobility, Delivery and Fate of optimized NPs under Field Relevant Conditions). According to UV-VIS spectroscopy in diffuse reflectance mode, the dominant fraction of iron is present as isolated Fe(III) species coordinated to the ion exchange sites of the zeolite with a certain fraction of small iron oxide clusters. Trap-Ox Fe-zeolites have a high SiO_2/Al_2O_3 ratio which provides rather hydrophobic channel surfaces for optimal adsorption of organic contaminants. Further properties of Trap-Ox Fe-zeolites are summarized in Table 4.
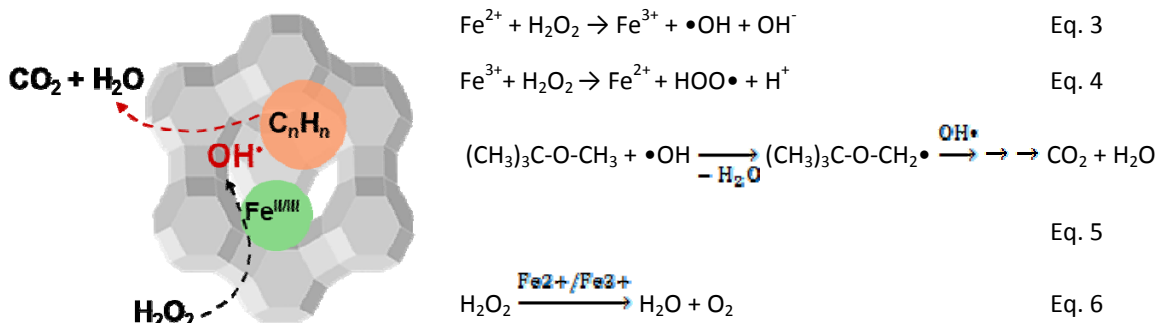
Table 4:   Overview of physico-chemical properties and reactivity parameters of Trap-Ox Fe-zeolites

Characteristics of Fe-Zeolites	Trap-Ox Fe-BEA35	Trap-Ox Fe-MFI120
Short description	Microporous alumosilicate particles loaded with iron ions which act as adsorbent and oxidation catalyst	
Mode of action	Adsorption of organic contaminants and activation of hydrogen peroxide for OH-radical-driven oxidation of a wide range of organic contaminants	
General chemical composition	$Fe^{3+}_n [(AlO_2)^-_x (SiO_2)_y] \cdot z H_2O$	
Elemental composition	Al: 20 g/kg Si: 360 g/kg Fe: 13 g/kg Molar ratio SiO_2/Al_2O_3 = 35	Al: 7.4 g/kg Si: 440 g/kg Fe: 3 g/kg Molar ratio SiO_2/Al_2O_3=120
Particle size [nm] (Z-average, DLS, 10 mM KNO_3 pH 8.3, 1 g/L particle concentration)	550	490
Specific surface area [m^2/g]	630	470
Maximum zeolite channel diameter [nm]	0.56	0.75
Density [g/cm^3] (calculated effective particle density with water-filled pores)	2.1	2.4
Sedimentation rate [nm/min]/Duration of suspension stability [days]	n.a./ stable suspension for 2 h at $c_{Fe-zeolite}$ = 10 g/L	
Zeta potential [mV]	-30.4 (F.I.s; pH 8.3)	-31.5 (F.I.s; pH 8.3)
pH of suspension	Native pH of suspensions is sightly acidic and adjusted to pH 8 - 8.5 for optimal suspension stability and parti-	

	cle transport	
Reactivity data (MTBE)	$A_{zeol,MTBE}$ = 0.025 L/g/h $A_{zeol,H2O2}$ = 0.011 L/g/h ($c_{Fe\text{-}zeolite}$ = 50 g/L, c_{MTBE} = 500 mg/L, c_{H2O2} = 8 g/L, medium: F.I.s, pH 8.2)	$A_{zeol,MTBE}$ = 0.11 L/g/h $A_{zeol,H2O2}$ = 0.0030 L/g/h ($c_{Fe\text{-}zeolite}$ = 10 g/L, c_{MTBE} = 100 mg/L, c_{H2O2} = 8 g/L, medium: F.I.s, pH 6.5)
Expected side-reactions	Gas formation (O_2, CO_2) upon contact of Fe-zeolite with H_2O_2 Uptake of cations (mainly divalent) from groundwater Very low leaching of Fe, Si, Al	
Type of stabilizers (in suspension)	No stabilizers needed in suspension with $c_{Fe\text{-}zeolite}$ = 10 g/L	
Expected products after aging	Zeolite with lower Si/Al ratio (if aging in slightly alkaline groundwater) and lower Fe^{3+} content	

5.3.2 Reactivity of Fe-zeolites

The iron in the zeolite pores (i.e. close to the adsorbed contaminants) is able to produce reactive species (e.g. hydroxyl radicals) from hydrogen peroxide, which degrade the contaminants. In analogy to the well-known Fenton reaction (Eq. 5 and 6), the Fe in the zeolite is supposed to change between its oxidation states +2/+3 in a catalytic cycle (Gonzalez-Olmos et al. 2013).

$$Fe^{2+} + H_2O_2 \rightarrow Fe^{3+} + \bullet OH + OH^- \qquad \text{Eq. 3}$$

$$Fe^{3+} + H_2O_2 \rightarrow Fe^{2+} + HOO\bullet + H^+ \qquad \text{Eq. 4}$$

$$(CH_3)_3C\text{-}O\text{-}CH_3 + \bullet OH \xrightarrow[-H_2O]{} (CH_3)_3C\text{-}O\text{-}CH_2\bullet \xrightarrow{OH\bullet} \rightarrow \rightarrow CO_2 + H_2O$$

$$\text{Eq. 5}$$

$$H_2O_2 \xrightarrow{Fe2+/Fe3+} H_2O + O_2 \qquad \text{Eq. 6}$$

Figure 13: Left: Scheme of contaminant adsorption and degradation within Fe-zeolite channels (modified structure based on Baerlocher and McCusker 2016), Right: Equations of most important involved reactions

The hydroxyl radicals produced are highly reactive and unselective and thus can react with a wide range of organic compounds leading to oxidized products of higher biodegradability (small organic acids) or even complete mineralization as shown exemplarily for MTBE in (Eq. 7). In the absence of organic compounds, hydrogen peroxide decomposition results in the formation of O_2 and H_2O (Eq. 8). Oxygen formation will be a side reaction also in the presence of organics.

Adsorption properties of Trap-Ox Fe-zeolites

Methyl *tert*-butyl ether (MTBE) was studied as one of the main target contaminants for Trap-Ox Fe-zeolites since it is a frequently occurring groundwater contaminant (due to its use as fuel additive) and is hardly degradable by any other *in-situ* method than chemical oxidation. MTBE sorption isotherms with Freundlich isotherm fits are shown in Figure 14. In the range of low aqueous phase concentrations Trap-Ox Fe-MFI120 even outcompetes activated carbon with respect to its adsorption affinity. Sorption to Trap-Ox Fe-zeolites is very fast due to their low particle size. Sorption equilibrium of MTBE with Fe-BEA35 in a well agitated suspension is established within < 3 min.
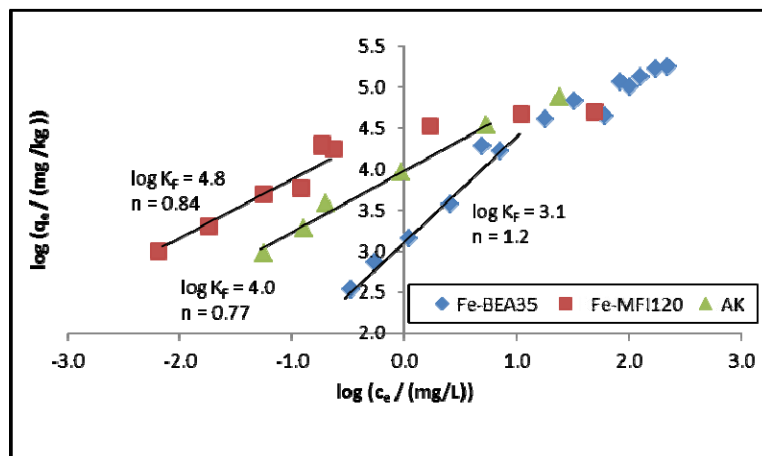
Figure 14: Sorption isotherms for model contaminant MTBE on two Trap-Ox Fe-zeolite types: Fe-MFI120 and Fe-BEA35 as well as activated carbon for comparison (F300, Chemviron), Freundlich coefficient K_F and constant n for the fitted concentration range (lines), medium: 10 mM KNO_3, pH 7.

Catalytic activity of Trap-Ox Fe-zeolites

Catalytic activity of Fe-zeolites was studied in batch and column experiments using standard water types (F.l.s and F.l.h) spiked with MTBE or a cocktail of model contaminants.
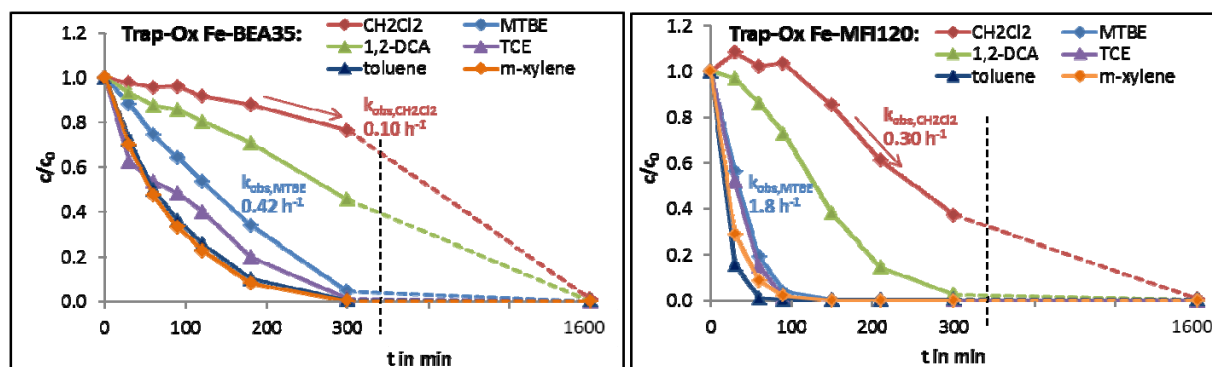
Figure 15: Degradation of a cocktail of model contaminants by H_2O_2 with two Trap-Ox Fe-zeolite types: Fe-BEA35 (left) and Fe-MFI120 (right), $c_{Fe\text{-}zeolite}$ = 10 g/L, $c_{0,cont}$ = 20 mg/L each, $c_{0,H2O2}$ = 8 g/L, medium: F.l.s, pH = 7.

Figure 15 shows the kinetics of degradation of various contaminants on Fe-MFI-120 and Fe-BEA35 including dichloromethane (CH_2Cl_2), 1,2-dichloroethane, trichloroethylene (TCE), toluene, m-xylene and MTBE in soft water (F.l.s) at pH 7.

All contaminants were completely degraded with one dosage of H_2O_2. The sequence in reactivity largely follows the expected reactivity with OH-radicals, electron-rich aromatic (m-xylene and toluene) and unsaturated compounds (TCE) are degraded fastest, compounds with e-withdrawing substituents (1,2-DCA and CH_2Cl_2) are degraded slowest.

In addition, MTBE adsorption and oxidation were studied in column experiments with Trap-Ox Fe-BEA35 using standard type water (F.l.h) spiked with MTBE (10 mg/L) and M.I as sand. After MTBE breakthrough, the adsorbed MTBE was oxidized by injection of H_2O_2 (10 g/L in F.l.h, pH 8.5) without any further additives. Trap-Ox Fe-BEA35 deposited on the sediment was active for MTBE adsorption and oxidation over the four tested adsorption/regeneration cylces with in total 320 exchanged pore volumes of water.

General application area

Application of Fe-zeolites in combination with H_2O_2 is an alternative to Fenton-like ISCO with dissolved iron. In the latter case, iron has to be kept in solution by applying large amounts of acid or complexing agents (EDTA, citric acid), otherwise iron would precipitate in the form of inactive iron oxyhydroxides at the near neutral pH of the aquifer. Fe-zeolites are active in a much wider pH-range (Table 4).

Thus, Trap-Ox Fe-zeolites can be injected in suspension together with the oxidant H_2O_2 for immediate oxidation of aqueous phase contaminants in the targeted aquifer zone at the native pH of the groundwater. In addition, due to their ability to adsorb organic contaminants, Trap-Ox Fe-zeolites can be used to form an *in-situ* sorption barrier after deposition on the aquifer sediment. This is highly desirable in case of extended and expanding plumes of contaminants where a sorption barrier can stop migration of contaminants and protects sensitive receptors. Furthermore, they act against rebound of aqueous phase contaminant concentrations which often occurs by matrix back diffusion of contaminants from dense or sorption-active aquifer sediments after an initial ISCO measure. In this case, Trap-Ox Fe-zeolites trap contaminants by adsorption, which stops any further migration and enriches contaminants in the zeolite pores close to the active iron sites for catalytic oxidation. Once that Trap-Ox Fe-zeolite was placed on the aquifer sediment, H_2O_2 solution can be injected for degradation of adsorbed contaminants without any additional activator/catalyst, which avoids any vigorous reactions (gas and heat production) known from injection of conventional Fenton reagents (i.e. dissolved iron salts + H_2O_2).

Hydroxyl radicals which are formed upon contact of Fe-zeolites and H_2O_2 react with almost all organic molecules. Therefore, Trap-Ox Fe-zeolites are applicable in cases where biodegradation or *in-situ* chemical reduction fails, e.g. in case of fuel oxygenates (MTBE, ETBE), halogenated aromatics (e.g. chlorobenzene) or halogenated alkanes (e.g. dichloroethane). However, fully halogenated molecules such as CCl_4 or perfluorinated surfactants (PFOA, PFOS) are some of the few examples which are expected to be hardly degradable by OH-radical driven oxidation including the Trap-Ox approach. Due to their narrow pores Trap-Ox Fe-zeolites add some selectivity to the radical-driven oxidation by virtue of size exclusion and adsorptive enrichment. Macromolecules such as natural organic matter

are excluded from access to the catalytic sites minimizing their impact as competitors for target contaminant degradation.

With respect to contaminant selectivity the two Trap-Ox Fe-zeolites are complementary (Table 5). Fe-MFI120 belongs to the group of hydrophobic MFI type zeolites (Gonzalez-Olmos et al. 2013) and is a high performance adsorbent for small organic molecules including many typical groundwater contaminants. Fe-BEA35 is a more universal adsorbent and catalyst allowing adsorption and degradation also for larger contaminant molecules.

Table 5:   Indications from bench scale studies for treatability by Trap-Ox Fe-zeolites/H2O2 application for common contaminant classes based on experimental results (compounds listed in parentheses in column 2) and prospective evaluation (classes marked with asterisks) based on chemical reactivity with OH-radicals and contaminant molecule size in relation to the zeolite pore size in Fe-BEA35 and Fe-MFI120

Contaminant classes	General treatability (in parentheses: compounds tested experimentally)	Applicable/Preferred Trap-Ox Fe-zeolite type
fuel oxygenates	very good (MTBE, ETBE, TBA)	Fe-BEA35 + Fe-MFI120
chlorinated ethenes	very good (TCE, PCE)	Fe-BEA35 + Fe-MFI120
halogenated ethanes	good (1,2 DCA), decreases with increasing halogen substitution degree	Fe-BEA35 + Fe-MFI120
halogenated methanes	good (CH_2Cl_2, $CHCl_3$), decreases with increasing halogen substitution degree	Fe-BEA35 + Fe-MFI120
BTEX	very good (benzene, toluene, o-xylene), but alternative method: bioremediation	both, but Fe-MFI120 limitations for larger substituents
halogenated aromatics and phenols	very good (chlorobenzene), decreases with increasing halogen substitution degree	both, but Fe-MFI120 limitations significant for high substitution degree
pharmaceuticals*	good for some (ibuprofen, diclofenac, carbamazepine), but to be tested individually	Fe-BEA35 (depending on molecule size)
surfactants*	good (Triton®, nonylphenol ethoxylate)	Fe-BEA35 (depending on molecule size)
aliphatic petroleum hydrocarbons**	to be tested	Fe-BEA35 (but limitations expected for highly branched and large cyclic aliphatics)
polycyclic aromatics**	to be tested	possibly Fe-BEA35 (but limitations expected for >3 ring PAHs)
polychlorinated biphenyls**	to be tested	possibly Fe-BEA35 (but limitations expected for highly substituted congeners)

* prospective evaluation, only a few representative compounds tested so far

** prospective evaluation, not tested so far

Table 5 summarizes treatability estimations for various compound classes based on experimental data (compounds listed in parentheses in column 2 of Table 5) and more generally, based on their known reactivity with OH-radicals and molecule sizes in relation to the pore size of the zeolite. Treatability for larger contaminants such as occurring typically among pesticides, pharmaceuticals, PAHs or PCBs remains to be tested on a case by case basis.

5.3.3   Influence of site conditions on particle applicability

Regarding site characteristics, as for nanoremediation in general, Fe-zeolites require a certain permeability of the subsurface in order to provide sufficient particle mobility. They are insensitive to the presence of oxygen in the groundwater and could hypothetically even be applied in unsaturated zones, e.g. for capturing soil vapour contaminations. The pH value of the groundwater has a minor influence on the adsorption properties of Trap-Ox Fe-zeolites but will influence their catalytic activity for H_2O_2 decomposition and contaminant oxidation. In this respect, the two Trap-Ox zeolites Fe-MFI120 and Fe-BEA35 behave differently. Fe-BEA35 has an applicable pH range from pH 5.5 to 8.5 with highest catalytic activity at pH 8.0 – 8.5. Fe-MFI120 is best applied at pH 5.5 – 7.0, since it has a low activity under alkaline conditions. Thus, selection of the most suitable zeolite type depends on the pH and also the buffer capacity of the groundwater. The presence of anions like sulphate, chloride or phosphate has a minor impact on catalytic activity of the Fe-zeolites. Uptake of divalent cations (Ca^{2+}, Mg^{2+}) in the zeolite pores can lead to lower degradation rates for sterically demanding contaminant molecules due to hindered mobility within the pores. Alkaline conditions favour slow dissolution of Si from the zeolite framework. Consequently, the long-term performance of Trap-Ox Fe-zeolites needs to be studied with the groundwater from the respective site. Results of batch and column tests on stability of Trap-Ox Fe-BEA35 under field-relevant conditions are described in detail in DL4.2. Based on these results it can be anticipated that after the injection and deposition on the porous medium, Trap-Ox Fe-BEA35 can actively adsorb and catalytically oxidize target contaminants (with H_2O_2 injections) for a period of at least two months under 'worst case' conditions (very hard water, pH 8.5, with NOM content).

5.4   Bionanomagnetite and Palladized Bionanomagnetite

Responsible partner: UMAN

5.4.1   Physico-chemical properties of bionanomagnetite

Microorganisms offer a sustainable and inexpensive route to synthesize nanoparticles that have catalytic properties and offer a benign solution to remediate a variety of target contaminants. Bionanomagnetite (Bnm) is one such nanoparticle that is synthesized by Fe(III)-respiring subsurface bacteria e.g. *Geobacter sulfurreducens* and *Shewanella oneidensis* (Lovley, 1987), in the presence of an electron donor such as lactate, acetate or hydrogen and an insoluble Fe(III) electron acceptor. We have also been testing a range of iron rich waste materials procured from members within the NanoRem

consortium, as an inexpensive feed for the biomagnetite synthesis. Recent studies show that bio-magnetite synthesis is scalable (Byrne et al., 2015, Muhamadali et al., 2015), and the physical proper-ties can be fine-tuned during bioproduction by controlling cell density and other parameters (Byrne et al. 2011), underpinning future commercial exploitation.

Newly synthesized Bnm has a thin layer of organic carbon residues on its surface, derived from lysed microbial cells (during biosynthesis), and it shows rapid aggregation and a high sedimentation rate. This can be controlled by the application of appropriate coatings. The following Table 6 illustrates the physicochemical properties of biomagnetite.

Table 6:   Overview of physical-chemical properties and reactivity parameters of Bionanomagnetite

Characteristics of Bionanomagnetite and Palladized Bionanomagnetite	
Short description	Nanosized, magnetite nanoparticles synthe-sized by bacteria
	Pd-Bnm biomagnetite with 5% mol Pd(0) on surface, effective catalyst in presence of H_2/formate as external electron donor
Mode of action	Reduction and sorption
	Pd Bnm reductive dehydrohalogenation
	and has been shown to reduce Cr(VI), Tc(VII), azo dyes and nitrobenzene
	Pd-Bnm: Cr(VI), Nitrobenzene, PCE
Chemical composition	Fe_3O_4 approx. 98 wt-%, some siderite also ob-served (XRD), Fe total: 72 wt% O: 28.8 wt%
Average primary particle size ± RDS [nm] (volume-based average particle size was de-termined by EyeTech™)	3.5 µm (although individual crystallites approx. 10-20 nm)
Specific surface area [m^2/g]	17.1 m^2/g (Watts et al., 2015); to be used with caution for interpretation of reactions as Bnm is susceptible to aggregation
Density [kg/m^3] (specify: true density, bulk density as powder, effective particle density with water-filled pores)	Not determined
Sedimentation rate [nm/min]	0.45 mm/hr
Zeta potential [mV] (specify: suspension fluid and pH)	+13 mV changes to -30 mV on storage
Type of stabilizers (in suspension)	No stabilizers used during synthesis and reac-tivity studies.
	For transport tests conducted later several stabilizers been used effectively
Content of stabilizers [%]	Only for transport studies
	2% agar and starch, 3% guar, sodium humate

	up to 1%
Zeta potential in presence of stabilizer [mV] (specify: suspension fluid and pH)	Guar -5.5 mV, agar -13.5 mV, starch -8.5 mV and humic salt of sodium -35 mV
Reactivity data towards target PCE	Biomagnetite shows poor reactivity against PCE but enhanced reactivity with palladized surface Pd-Bnm the k_{obs} (min^{-1}) is 0.265 (Pd-bnm 0.025 mg/L), PCE 50 mg/L, soft water F.I h and pH 6.8
Expected side-reactions	No side reaction, limited reactivity of Bnm (Fe^{2+} oxidized) Both Bnm and Pd Bnm passivate due to surface accumulation of Cr (III)
Expected products after aging	

5.4.2   Reactivity of Biomagnetite

Biomagnetite is highly reactive against redox active contaminants and can be used to reduce heavy metals and organic compounds into their less toxic forms. The following description illustrates the particle application areas, observations and associated limitations involving its use for reduction of the model contaminant Cr(VI).

Application 1: The potential use of Bnm for the remediation of Cr(VI)

This has been investigated initially by using model Cr(VI)-containing solutions in batch experiments (Cutting et al., 2010) and also column systems (Crean et al., 2012). Bnm is able to reduce and precipitate Cr(VI).

The reaction rate for the removal of Cr(VI) from model solutions was reported to be $0.71 \cdot 10^{-3}$ min^{-1} for Bnm, and 32 mg Cr(VI) was removed per gram of Bnm. A study by Watts et al. (2015) used chromite ore processing residue (COPR) from a site in Glasgow, UK. This is a significant pool of soluble Cr(VI) minerals (~10 g/kg) creating a hyper alkaline, high Cr(VI) (>1mM) leachate. Addition of Bnm (5 wt%) was shown to source stabilise the readily leachable Cr(VI) by reducing it to Cr(III). Bmn reduced a significant fraction of mineral bound Cr(VI), forming a product that was recalcitrant to air re-oxidation (Watts, Coker et al. 2014). For the COPR groundwater, the reaction rate (k_{obs}) was $1 \cdot 10^{-3}$ min^{-1}. Both samples tested for treatment were alkaline (at pH 12) (Figure 16).

Observations

Bnm is applicable across a wide pH range, including hyperalkaline samples, the only limitation being the passivation of the reactive surface of the Bnm. This occurs either due to oxidation of Fe(II) and subsequent formation of an Fe(III) capping layer, or the overgrowth of Cr(III) precipitates, which could act as a barrier to effective electron transfer from the Bnm to the contaminant.
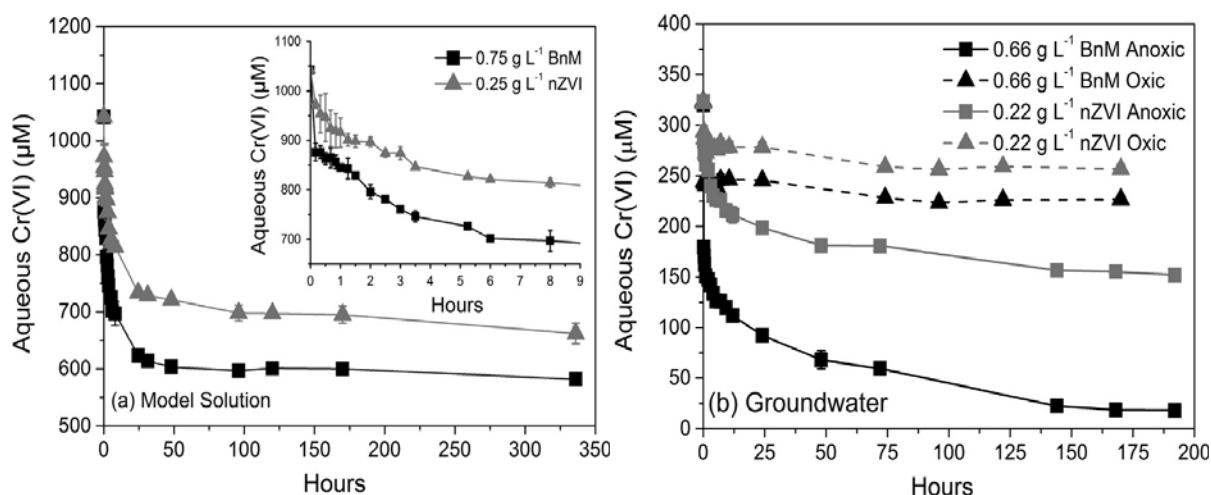
Figure 16: Aqueous Cr(VI) removal from a model pH 12 Cr(VI) solution (a) and a Cr(VI) contaminated groundwater (b) over time, when amended with Bnm or nZVI (NANOFER 25S). Inset graph (a) shows removal over the first 9 h of the reaction. Error bars represent the standard deviation of the triplicate values (Watts et al., 2015)

Application 2

Bnm has also been shown to reduce nitrobenzene rapidly and form aniline in this process (Figure 19) though the non-functionalized form of Bnm has limited reactivity against solvents such as PCE and TCE unless functionalized with Pd (see section below).

Application 3

Bnm has been shown to reduce the azo dye Ramazol Black B. This dye is a chemically stable, xenobiotic and usually not effectively degraded by the conventional chemical techniques, but the addition of Bnm reduced the azo chromophore component of the dye, rapidly forming the corresponding amines (Pattrick et al., 2013).

Bnm is also currently being tested against nuclear contaminants such as Tc(VII) and Np(V) which are reduced very efficiently to Tc(IV) and Np(IV) respectively.

5.4.3   Influence of site conditions

Based on the reduction studies, the Bnm is stable and efficient to remediate wastes such as Cr(VI) at pH 7-12. Although Bnm has not been applied in field-scale applications, it has been planned to test sediments from brownfield sites from Portugal, Spain and the UK, which have challenging heavy metal profiles with high concentrations of metals such as Cr, As and Cu. The presence of oxygen is detrimental towards the reactivity of Bnm as it largely depends on the Fe(II) content of Bnm.

Palladized biomagnetite (Pd-Bnm)

Pd-Bnm has been used to remediate a broad range of toxic contaminants, with the Pd-coating used as an electron delivery system for reductive processes. The reactivity of Bnm is driven by Fe^{2+} (fer-

rous) in the chemical structure (and reactive surface) which is subsequently oxidized to ferric (Fe^{3+}) during the reduction of contaminants. This exhausts the reduction potential of Bnm for remediation applications. The aim behind synthesis of palladized Bnm was to generate a catalytically reactive, inexhaustible heterostructure that could facilitate continual reactivity and reduce substrates in the presence of external electron donors such as hydrogen and formate ions.

General application areas

Cr (VI) remediation

Reactivity of Pd-Bnm was tested against Cr(VI) in batch reactor experiments, using model chromium (VI) solutions. Hexavalent chromium is extremely toxic with an upper permissible limit of 50 ppb (World Health Organization) for water samples. H_2 or sodium formate was used as the external electron donors in these studies (Cutting et al., 2010). This study was further extended to treat field samples obtained from a site in south east Glasgow, UK, contaminated with chromite ore processing residues (COPR) (Watts, Coker et al. 2015). It was observed that in the presence of H_2 as electron donor, this system achieved a high removal of Cr(VI) (up to 700 mg / g catalyst) from model solutions prior to catalyst deactivation due to overgrowth by the reduced Cr(III). In addition 200 mM formate was also used as electron donor with model Cr solution and COPR leachates (Figure 17).
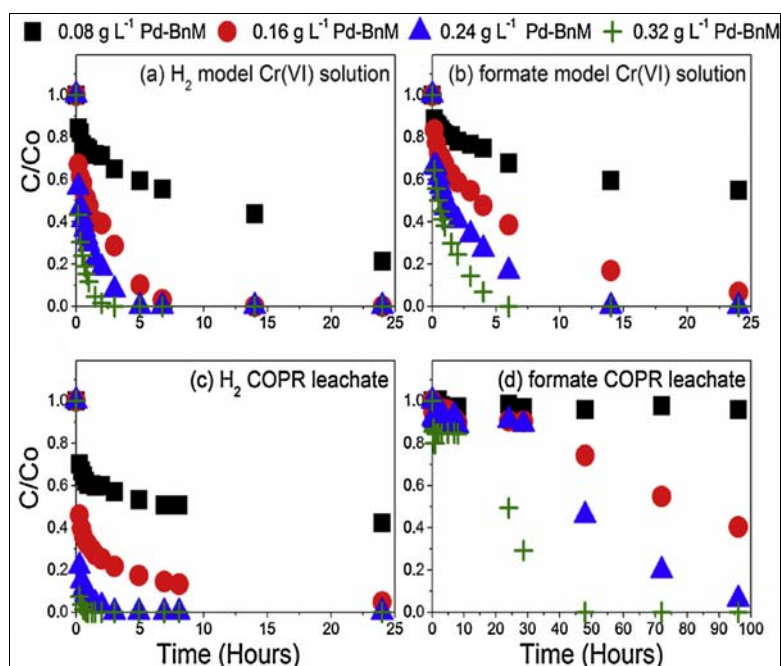
Figure 17: c/c_0 of aqueous Cr(VI) over time with Pd-BnM/H_2 gas in a model 0.5 mM Cr(VI) solution (a) and 0.5 mM Cr(VI) COPR leachate (c), and Pd-BnM/100 mM formate in a model Cr(VI) solution (b) and COPR leachate (d). Different time scale were used for (d) (Watts et al., 2015 b)

The Cr(VI) removal rate from COPR leachate was low in Pd-Bnm-formate systems. It was difficult to model the data using pseudo-1st order reaction rates. Figure 18 shows the rate constants for Cr(VI) removal in the batch studies.
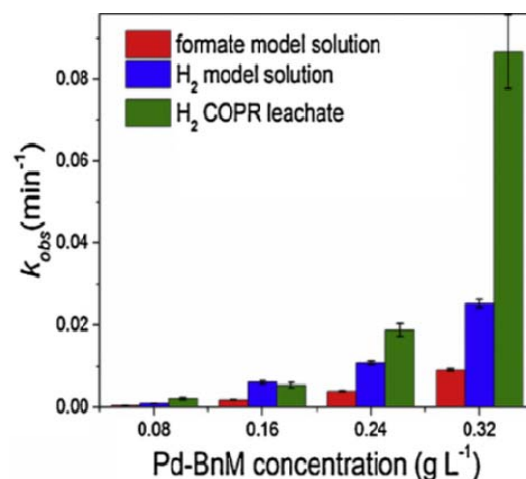
Figure 18: Pseudo-1st order reaction rate constants, k_{obs} (mins^{-1}), of aqueous Cr(VI) removal with varying electron donor and reaction solution (Watts et al., 2015).

Application of Pd-Bnm for remediating organic compounds

Palladized-Bnm has also been tested for its potential to reduce and degrade nitrobenzene (ArNO$_2$) and perchloroethylene (PCE). It was able to degrade nitrobenzene and this reaction was accompanied by formation of aniline. Similarly, PCE was rapidly dechlorinated and ethane was released. The details are discussed below.

Batch reactor study for nitrobenzene

The Bnm was diluted in 20 mM MOPS buffer (30 mL in a 50 mL serum bottle). It was purged with N$_2$ gas and 150 µM nitrobenzene was added. The samples were collected and analysed by HPLC. It was observed that at the end of reaction approximately 140 µM aniline (Figure 19) was formed but its rate of formation was slow, suggesting formation through unknown intermediates.
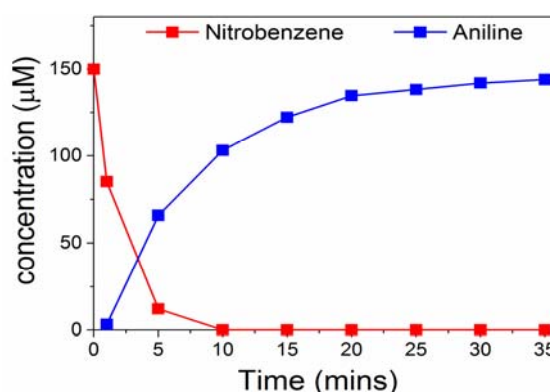
Figure 19: Reactivity of Bnm towards nitrobenzene and formation of aniline

15% Pd-Bnm was also used in similar batch experiments; except that the headspace was purged with H$_2$ and five spikes each of 1mM nitrobenzene were added. Concurrent removal of nitrobenzene and production of aniline occurred as shown in Figure 20.
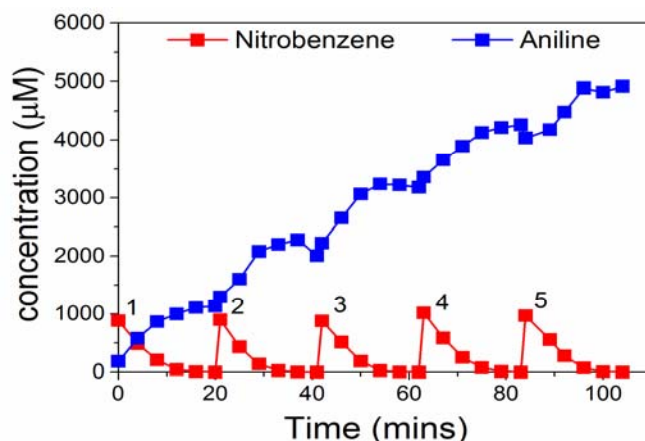
Figure 20: Concentration of contaminant nitrobenzene and accumulation of the reduced product aniline as a function of time in presence of Pd-Bnm for several reaction cycles. The number annotations refer to the repeated spiking of the batch experiment with 1mM nitrobenzene.

Batch reactor studies for remediation of PCE

The reactivity of both Bnm and Pd-Bnm was investigated according to the harmonized protocol described in IDL 4.1. A synthetic groundwater was prepared (IDL 4.1) and purged with N_2, leaving a volumetric ratio of 1:1 liquid and headspace (pH 6.8 during the reaction). The headspace was purged with H_2. The concentrated PCE stock with hexane as internal standard was added, to a final concentration of 50 mg/L total PCE as the starting concentration.

The Bnm and Pd-Bnm were added to reaction vessels to a final concentration of 1 g/L and 0.025 g/L (Fe) respectively. The batch reactions were mixed and left to equilibrate and headspace analysis was done for both, PCE and intermediates, by GC-FID. It was observed that with 1 g/L Bnm the reaction rate was very slow, however with Pd-Bnm the PCE was degraded rapidly with ethane formed as an end product (Figure 21).
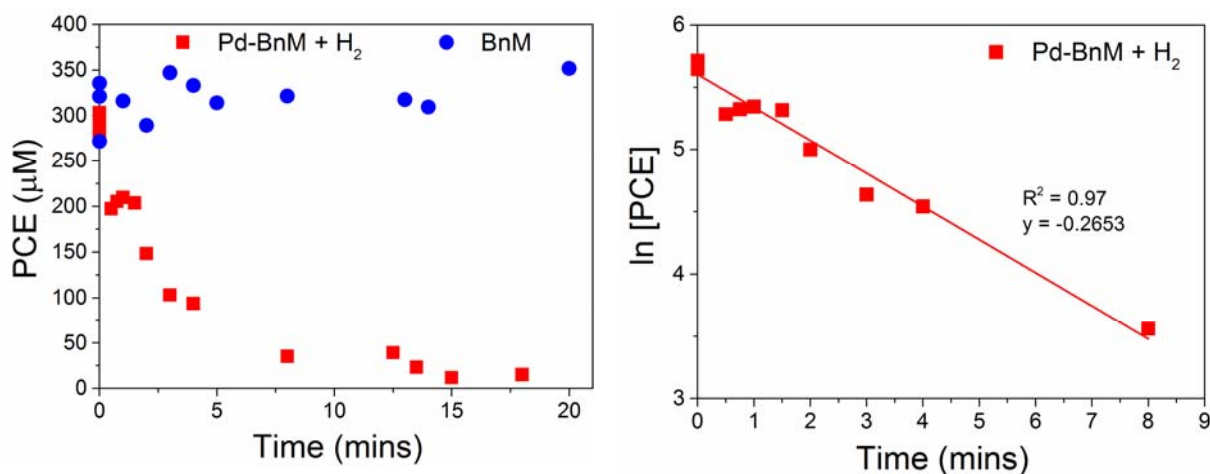
Figure 21: PCE dechlorination kinetics of the Pd-Bnm in the presence of H_2. Left: PCE concentration for the synthetic groundwater treated with Bnm (blue circles, 1 g L^{-1} Fe) and 5%-Pd-Bnm

(0.025 g L^{-1} Fe) supplied with an excess of H$_2$ gas (red squares). Right: Linear regression of ln[PCE] vs. time used to calculate k_{obs}.

Table 7:   Reaction kinetics for the dechlorination of PCE by Pd-Bnm.

Catalyst	Pd g L^{-1}	K_{obs} (min^{-1})	R^2	K_{Pd} (L g$_{Pd}^{-1}$ min^{-1})	A_{Pd} (L g$_{Pd}^{-1}$ min^{-1})
Pd-BnM	7.94 x 10^{-4}	0.265 $\pm$ 0.014	0.97	334 $\pm$ 18	492 $\pm$ 25

5.5   Non-ZVI metals (Mg/Al particles)

Responsible partner: USTUTT

5.5.1   Physical-chemical properties of non-ZVI metals

Zero-valent iron particles have been reported to be capable of degrading a wide variety of contaminants, such as chlorinated hydrocarbons (Suresh, 2009). Here, the reactivity of Al and Mg towards the model contaminant PCE has been investigated since Al and Mg offer a better stoichiometry compared to iron. Accordingly, 1.34 g Fe^0 would be required for the degradation of 1 g PCE to ethene but only 0.59 g Mg^0 and 0.43 g Al^0, respectively. Commercially available microparticles have been used for the reactivity tests. The Al particles (d_{50} = 1.8 µm) had a spherical shape (see Figure 22) and a specific surface area of 1.8 m^2/g. The specific surface area of the Mg microparticles was 6.4 m^2/g. Aluminium/magnesium metal alloy particles (Al:Mg = 1:1) having a particle size of approx. 100 µm (producers data) and a specific surface area of 0.2 m^2/g have also been investigated. Physical-chemical properties of non-ZVI metals are summarized in

Table 8.
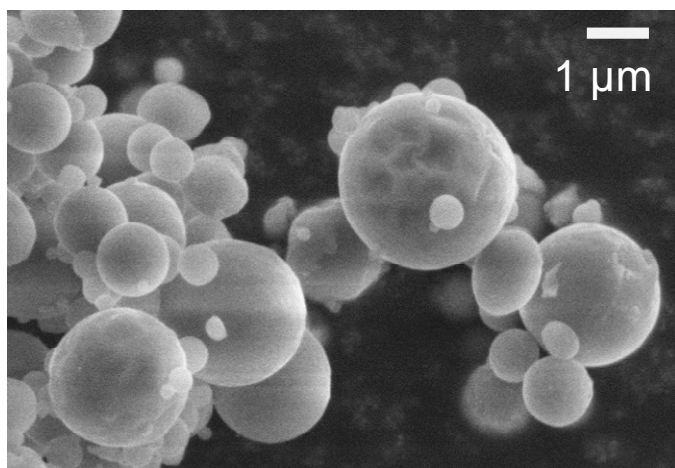
Figure 22: ESEM micrograph of Al particles (MPA, University of Stuttgart)

Table 8:   Overview of physical-chemical properties of non-ZVI metals

Characteristics of non-ZVI metals	Al	Mg	Al/Mg
Short description	Al^0 microparticles	Mg^0 microparticles	Al/Mg alloy
Mode of action	Chemical reduction		
Chemical composition	Al(0) ≈ 100% Trace elements: Fe	Mg(0) = 98.8% Trace elements: Fe, Al	Al: 48-52%[a] Mg: 48-52%
Average primary particle size [µm] (SLS)	d_{10} = 0.8 d_{50} = 1.8 d_{90} = 3.6	d_{10} = 12.8 d_{50} = 28.8 d_{90} = 54.7	n.d.
Specific surface area [m^2/g]	1.8	6.4	0.2
Density [kg/m^3]	900-1200[a] (bulk density)	n.a.	≈ 900[a] (bulk density)
Sedimentation rate [nm/min]	n.a.	n.a.	n.a.
Zeta potential [mV]	n.a.	n.a.	n.a.
pH of suspension	n.a.	n.a.	n.a.
Reactivity data towards target PCE	See Table 13	n.a.	See Table 13
Expected side-reactions	Anaerobic corrosion (hydrogen evolution)		
Type of stabilizers (in suspension)	n.a.	n.a.	n.a.
Expected products after aging	Hydroxides		

[a] Producer's data.

5.5.2   Reactivity of non-ZVI metals

Reactivity towards the main target contaminant PCE was investigated in column experiments under flow-through, and thus field similar conditions. Using Mg microparticles chloride formation was neglectable. As a consequence of anaerobic corrosion a strong hydrogen formation was observed; pH values between 11 and 12 were measured throughout the experiment. Mg is therefore not suitable for PCE degradation.

$$Mg + 2\ H_2O \rightarrow Mg^{2+} + 2\ OH^- + H_2 \hspace{4cm} Eq.\ 7$$

For pure Al a low chloride formation was found. PCE degradation could be improved using mechanically activated Al particles (by ball milling them together with Al_2O_3 prior to use, Petrovic et al., 2010) (see Table 9). Al/Mg metal alloy particles also showed a higher PCE degradation in terms of chloride formation compared to Al.

Table 9:   Non-ZVI metals: determination of PCE degradation and anaerobic corrosion[a]

	PCE → Cl⁻ [%]	PCE → TCE [%]	$m_{corroded\ Al(0)}/m_{overall\ consumed\ Al(0)}$ [%]
Al	7	1.5	97
Mechanically activated Al particles	49	0.5	70
Al/Mg	53	0.1	n.d.

[a] The duration of the experiment was 41 days.

Using mechanically activated Al particles a low amount of TCE (<< 1 mg/l) was formed between days 7 and 25 of the experiment. For Al/Mg metal alloy particles only traces of TCE were found. Traces of *cis-* and *trans*-DCE were found for both particles, but no VC. Ethene/ethane were detected as final degradation products.

With regard to the general application areas of the investigated particles, results indicate that Mg is not suitable for the degradation of chlorinated ethenes (PCE), chlorinated ethanes (1,2-DCA, HCA) and perchlorate. Al showed a poor PCE degradation in column tests. The use of mechanically activated Al particles and Al/Mg particles resulted in a higher PCE degradation. However, chloride formation was most pronounced within the first 2-3 weeks of the experiment (see Figure 23).
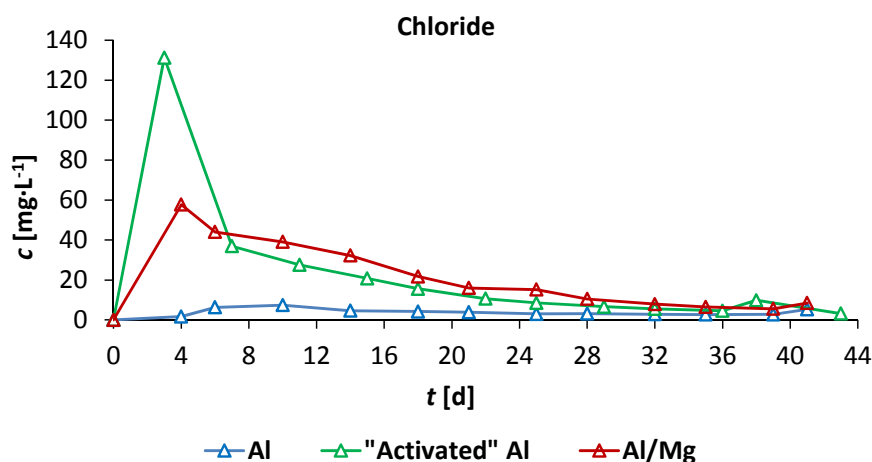
Figure 23: Non-ZVI metals: chloride formation

Batch tests showed that Al is not suitable for the degradation of chlorinated ethanes (1,2-DCA, HCA). Neither for Al nor for Al/Mg a reduction in perchlorate concentration was found.

5.5.3   Influence of site conditions on particle applicability

Lab-scale tests focusing on PCE as target contaminant have been performed. Results of column tests showed that pollutant degradation could be improved by using mechanically activated Al particles or an Al/Mg alloy. However, taking into account the observed long-term reaction behaviour, Al-based particles seem to be rather inappropriate for any large-scale application. In any case aerobic media as well as strong acidic media should be avoided to prevent oxidation of the metals.

5.6   Barium Ferrate

Responsible partner: USTUTT

5.6.1   Physical-chemical properties of barium ferrate

The past decade showed a significant increase in publications about the use of ferrates(VI) for "super-iron" batteries or wastewater treatment. Under acidic conditions, ferrate(VI) has the highest redox potential of any oxidant used in water and wastewater treatment (Jiang et al., 2002). Under alkaline conditions, however, ferrate(VI) is a relatively mild oxidant (Ghernaout et al., 2011).

$$FeO_4^{2-} + 8\ H^+ + 3\ e^- \rightarrow Fe^{3+} + 4\ H_2O \qquad\qquad E^0 = 2.20\ V \qquad\qquad\qquad Eq.\ 8$$

$$FeO_4^{2-} + 4\ H_2O + 3\ e^- \rightarrow Fe(OH)_3 + 5\ OH^- \qquad\quad E^0 = 0.72\ V \qquad\qquad\qquad Eq.\ 9$$
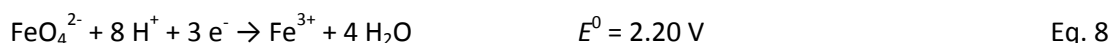
Its barium salt ($BaFeO_4$) offers slow-release properties and could hence be utilized to create a depot-effect in the aquifer. Preparation of $BaFeO_4$ has been focusing on an *ex-situ* electrochemical synthesis

route in which $BaFeO_4$ is obtained by subsequent precipitation of electrochemically prepared FeO_4^{2-} (Licht et al., 2004)

$$Fe + 2\ OH^- + 2\ H_2O \rightarrow FeO_4^{2-} + 3\ H_2 \qquad\qquad \text{Eq. 10}$$

$$FeO_4^{2-} + Ba^{2+} \rightarrow BaFeO_4 \qquad\qquad \text{Eq. 11}$$

Figure 24: $BaFeO_4$ sample

UV-Vis spectra showed the distinctive absorption maxima of FeO_4^{2-} at around 500 and 800 nm (Tiwari et al., 2011). Titrimetric chromite analysis revealed an Fe(VI) content of 40-60% depending on batch. Qualitative characterization by X-ray diffraction (XRD) (see Figure 25) showed that main impurities are caused by carbonate species.
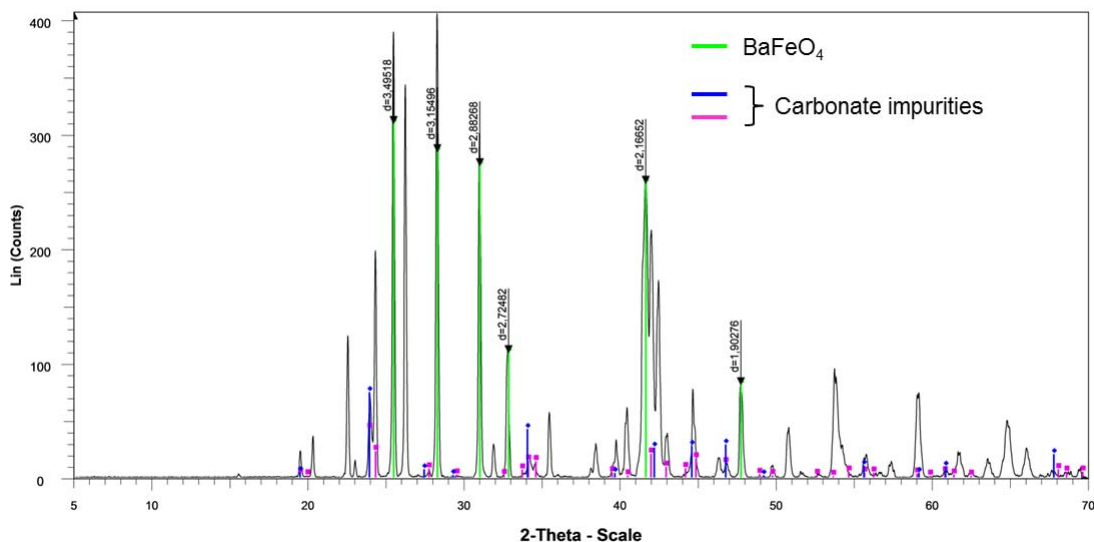
Figure 25: XRD spectrum (MPA, University of Stuttgart) showing the $BaFeO_4$ pattern in good agreement with Licht et al. (Licht et al., 2001) as well as the presence of carbonate impurities

With regard to the preparation of $BaFeO_4$ yield has therefore still to be improved by minimizing by-products; there is no final product available yet. In order to investigate the reactivity of the obtained products towards toluene batch tests have been performed (see 5.6.2). Physical-chemical properties of $BaFeO_4$ are summarized in Table 10.

Table 10: Overview of physical-chemical properties of barium ferrate

Characteristics of Barium Ferrate	
Short description	Ferrate(VI)
Mode of action	Chemical oxidation
Chemical composition	Fe(VI) = 40-60% (depending on batch) (No final product available yet.)
Average primary particle size ± RDS [nm]	n.a.
Specific surface area [m^2/g]	n.a.
Density [kg/m^3]	n.a.
Reactivity data towards target toluene	See Table 13
Expected side-reactions	Decomposition of ferrate in water (formation of oxygen) (Murmann et al., 1974)
Expected products after aging	Ferric hydroxide

5.6.2   Reactivity of Barium Ferrate

The oxidation of BTEX contaminants by means of $BaFeO_4$ has been investigated in batch tests using toluene as model contaminant. A decrease in toluene concentration of about 20% was found after 2 weeks reaction time (see Figure 26) ($k_{obs} = 7.6 \cdot 10^{-4}$ h^{-1}). Traces of benzaldehyde and benzoic acid were detected. Under acidic conditions (pH 2) a reduction in toluene concentration of 60% was found in the same period of time ($k_{obs} = 2.8 \cdot 10^{-3}$ h^{-1}). As intermediates benzaldehyde (traces) and benzoic acid (toluene → benzoic acid: > 7%) were detected. Batch reactivity tests proved that strong acidic conditions favour toluene degradation which is considered to be of limited practical relevance. Moreover, pollutant degradation seems to be limited by the low concentration of FeO_4^{2-} resulting from the low solubility of $BaFeO_4$. As a result current experiments are focusing on the use of $BaFeO_4$ for stimulating the microbial degradation of 4-nitrotoluene (by providing an electron acceptor).
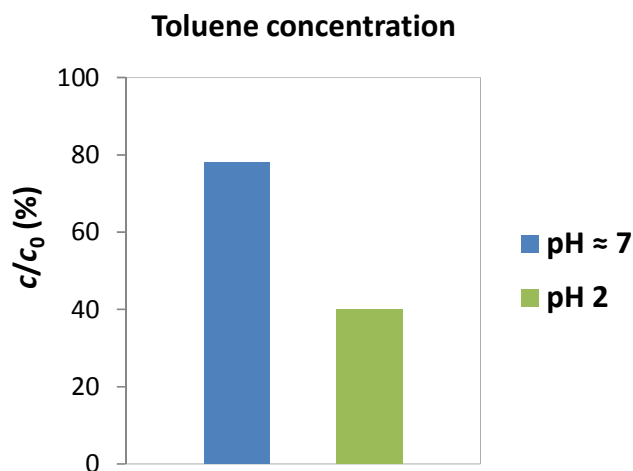
Figure 26: Reactivity of BaFeO$_4$ towards toluene in batch tests (reaction time 2 weeks, c_0 = 54 mg/L, $n_{\text{ferrate(VI)}}/n_{\text{toluene}} \approx 1.5/1$)

5.6.3   Influence of site conditions on particle applicability

Barium ferrate is at the state of laboratory development. Preliminary results of batch reactivity tests focusing on the potential use of BaFeO$_4$ for the degradation of BTEX contaminants using the example of toluene indicate that BaFeO$_4$ is not applicable for large-scale applications.

6   Summary and Overview of Particles Abilities and their Application area

Table 11: Overview of identified application areas/potential of particles

Particle Type	Reaction types supported by the particles							Reaction mode				Recommendation for site conditions					Stabilizer needed		General rules for use				Possible spin-off applications			Development status		
	Oxidation	Reduction	Hydrophobic sorption	Sorption of metals/metalloids	Support of biology. treatment	Hydrolysis		Reactive compon. consumed	Additional reagents needed	Gaseous products formed		Anaerobic	Aerobic	pH << 7	pH ≈ 7	pH > 7	yes	no	Inertization of susp. needed	Disperser needed			wastewater			Tested at field scale	Ready for up-scaled testing	Research at laboratory scale
Nano-Goethite	X			X	X												X											
Carbo-Iron	(X)	X	X	X	X	(X)		X		X		X			X	X	X		X	X			X			X		
Trap-Ox Fe-BEA35	X		X						X	X		X	X		X	X		X		X			X				X	
Trap-Ox Fe-MFI120	X		X						X	X		X	X	X	X			X		X			X					X
Bionanomagnetite (Bnm)		X		X								X			X			X		X			X					X
Pd-Bnm		X		X						X		X			X	X		X		X			X					X
Al, Mg		X						X	(X)	X		X			X	X												X
BaFeO$_4$	X							X		X		X	X	X	X								X					X

Table 12: List of selected contaminants degradable (+ successfully tested, - not applicable, L likely, but not tested), adsorbed or otherwise treatable (t)

Particle Type	Chlorinated Olefins (e.g.C2Cl4, C2HCl3, C2H2Cl2)	Brominated Olefins (e.g. C2H3Br)	Halomethanes (e.g. CCl4, CHBr3, CHBr2Cl ...)	Saturated polyhalogenated (e.g. C2H3Cl3)	Dichloroethane, Dichloromethane	Aromatics, Phenols (low substitution degree, e.g. dichlorobenzene)	Aromatics, Phenols (high halogenation degree, e.g. PCBs, Pentachlorophenol)	Herbicides and pesticides (e.g. DDT, Lindane)	Pharmaceuticals (e.g. Iopromid)	BTEX	PAHs	Fuel oxygenates (MTBE, ETBE)	Petroleum hydrocarbons	Metals/Metallois (e.g. Cr(VI), Cd(II), As(II))	Nitro compounds (e.g. TNT, nitrobenzene)	Perchlorate	Further contaminants tested [1]
Nano-Goethite	-	-	-	-	-		L	-		+	L	L	L	t	L		
Carbo-Iron	+	+	+	+	-	-	L	L	L	t	t		t	t	L	L	
Trap-Ox Fe-BEA35	+	L	+/-[2]	+	+	+	L	L	+/-[3]	+	L/-[3]	+	L	-	L	-	Triton-X100
Trap-Ox Fe-MFI120	+	L	+/-[2]	+	+	+	-	-	-	+	-	+	L/-	-	L	-	+
Bionanomagnetite (Bnm)														+	+		
Pd-Bnm	+																Rama-zol
Al	+		L	-	-											-	
Al/Mg	+		L													-	
BaFeO₄						L				+					L		

[1] Further substances are listed in the individual particle descriptions in chapters 3.1 to 3.7; [2] not applicable for CCl₄, [3] depending on molecule size

Table 13:   Reactivity data for typical target contaminants

NPs	NP concentration [g L^{-1}]	Contaminant	Initial contaminant concentration [mg L^{-1}]	Type of background solution	pH of background solution	Contaminant degradation		Corrosion	Fe^0 efficiency	Additional data
						k_{obs} [h^{-1}]	k_{SA} [L m² h^{-1}]	k_{H2} [h^{-1}]	$\in$ [%]	
Nano-Goethite	1	Toluene	20	F.I.S	6.5	$1.9x10^{-2}$				0.47 µM/day
	1	Benzoate	72	F.I.S	5	7.75×10^{-2}				1.86 µM/day
Carbo-Iron®	1	PCE	50	F.I.m	7.6	7.6×10^{-3}	1.3×10^{-3}	2.1×10^{-3}	5.2	
Trap-Ox Fe-BEA35	50	MTBE	500	F.l.s	8.2	1.3				with $C_{H2O2,0} = 8$ g L^{-1}: $A_{zeol,MTBE} = 0.025$ L g^{-1} h^{-1}
Trap-Ox Fe-MFI120	10	MTBE	100	F.l.s	6.5	1.1				$A_{zeol,MTBE} = 0.11$ L g^{-1} h^{-1}
Bionanomagnetite (Bnm)	0.75	Cr	46.8	Deion. water +NaOH	12	0.066	$3.85x10^{-5}$			$A = 1.1×10^{-3}$ L g$_{NP}^{-1}$ min^{-1}
Pd-Bnm	0.32	Cr	46.8	Deion. water +NaOH	12	1.5				Non-linear at high concentration
Al (Column)		PCE	≈ 55 mg/L	F.II	≈ 8	3.1×10^{-3}				Dechlorination (41 d): PCE → Cl$^-$: 7%, PCE → TCE: 1.5% Traces of DCE Anaerobic corrosion (41 d): $m_{corroded\,Al(0)}/m_{overall\,consumed\,Al(0)}$: 97%
Al/Mg (Column)		PCE	≈ 55 mg/L	F.II	≈ 8					Dechlorination (41 d): PCE → Cl$^-$: 53% Traces of TCE + DCE
BaFeO$_4$ (Batch)		Toluene	54	Deion. water	<u>≈7</u>	7.6×10^{-4}				Ferrate(VI)/toluene ≈ 1.5/1 (mol/mol)

List of References

Bleyl, S., F.-D. Kopinke, Mackenzie, K. (2012). Carbo-Iron®—Synthesis and stabilization of Fe(0)-doped colloidal activated carbon for in-situ groundwater treatment. Chem. Engin. J., 191, 588-595.

Bosch J., Heister K., Hofmann T., Meckenstock R.U. (2010) Nanosized iron oxides strongly enhance microbial iron reduction. Appl. Environ. Microbiol., 76, 184-289.

Byrne, J. M., Muhamadali, H., Coker, V. S., Cooper, J., Lloyd, J. R. (2015) Scale-up of the production of highly reactive biogenic magnetite nanoparticles using Geobacter sulfurreducens. J. R. Soc. Interface, *12*(107), 20150240, doi:10.1098/rsif.2015.0240.

Byrne, J. M., Telling, N. D., Coker, V. S., Pattrick, R. a. D., Van Der Laan, G., Arenholz, E., Tuna, F., Lloyd, J. R. (2011) Control of nanoparticle size, reactivity and magnetic properties during the bioproduction of magnetite by Geobacter sulfurreducens. Nanotechnol. 22, 455709.

Baerlocher, C., McCusker, L.B., Database of Zeolite Structures: http://www.iza-structure.org/databases/

Coker, V. S., Bennett, J. A., Telling, N. D., Henkel, T., Charnock, J. M., Van Der Laan, G., Pattrick, R. a. D., Pearce, C. I., Cutting, R. S., Shannon, I. J., Wood, J., Arenholz, E., Lyon, I. C., Lloyd, J. R. (2010) Microbial Engineering of Nanoheterostructures: Bio-logical Synthesis of a Magnetically Recoverable Palladium Nanocatalyst. ACS Nano 4, 2577-2584.

Crean, D. E., Coker, V. S., Van Der Laan, G., Lloyd, J. R. (2012) Engineering Biogenic Magnetite for Sustained Cr(VI) Remediation in Flow-through Systems. Environ. Sci. Technol. 46, 3352-3359.

Cutting, R. S., Coker, V. S., Telling, N. D., Kimber, R. L., Pearce, C. I., Ellis, B. L., Lawson, R. S., Van Der Laan, G., Pattrick, R. a. D., Vaughan, D. J., Arenholz, E., Lloyd, J. R. (2010) Optimizing Cr(VI) and Tc(VII) Remediation through Nanoscale Biomineral Engineering. Environ. Sci. Technol. 44, 2577-2584.

DL 4.1; Wagner, S., Micic Batka, M.V.V., Schmid, D., Hofmann, T. (2015) NanoRem Deliverable DL 4.1 on Initial particle stability, mobility and deliv-ery: Report on the stability, mobility, and en-hanced delivery of NPs that are accessible at the beginning of the project.

DL 4.2; Hoffmann, T. Micic Batka, M.V.V. (2016) NanoRem Deliverable DL 4.2 on Stability, Mobility, Delivery and Fate of op-timized NPs under Field Relevant Conditions.

Elimelech, M., Gregory, J., Jia, X., Williams, R. A. (1995). Particle Deposition & Aggregation. Woburn, Butter-worth-Heinemann.

Elion, E., Elion, L. (1933) Eine einfache gasvolumetrische Methode. Z. Anal. Chem. 92, p. 89-92.

Fuchs, G., Boll, M., Heider, J. (2011) Microbial degradation of aromatic compounds – from one to four strategies. Nature Review 9, 803-816.

Georgi, A., Gillies, G., Mackenzie, K., Kopinke, F.-D. (2015) Extended Abstract, 5 Pages, Proceedings of Aqua-ConSoil 2015, 9–12 June, Kopenhagen http://www.aquaconsoil.org/ proceedings.html.

Ghernaout, D., Naceur, M.-W. (2011) Ferrate(VI): In situ generation and water treatment - A review. Desalin, Water Treat. 30, p. 319-332.

Gillies, G., Mackenzie, K., Kopinke, F.-D., Georgi, A (2016) Fluorescence labelling as tool for zeolite particle tracking in nanoremediation approaches. Sci. Tot. Environ. 550, 820-826.

Gonzalez-Olmos, R., Holzer, F., Kopinke, F.-D., Georgi, A (2011) Indications of the reactive species in a hetero-geneous fenton-like reaction using fe-containing zeolites. Appl. Catal. A: General 398, 44-53.

Gonzalez-Olmos, R., Kopinke, F.-D., Mackenzie, K., Georgi, A. (2013) Hydrophobic fe-zeolites for removal of MTBE from water by combination of adsorption and oxidation. Environ. Sci. Technol. 47, 2353-2360.

Hochella M.F., Lower S.K., Maurice P.A., Penn R.L., Sahai N., Sparks D.L., Twining BS (2008) Nanominerals, mineral nanoparticles, and Earth systems. Science 319, 1631–1635.

Jiang J.-Q., Lloyd B. (2002) Progress in the development and use of ferrate(VI) salt as an oxidant and coagulant for water and wastewater treatment. Water Res. 36, p. 1397-1408.

Licht S., Naschitz V., Halperin L., Halperin N., Lin L., Chen J., Ghosh S., Liu B. (2001) Analysis of ferrate(VI) compounds and super-iron Fe(VI) battery cathodes: FTIR, ICP, titrimetric, XRD, UV/VIS, and electrochemical characterization. J. Power Sources, 101, 167-176.

Licht S., Tel-Vered R., Halperin L. (2004) Toward Efficient Electrochemical Synthesis of Fe(VI) Ferrate and Super-Iron Battery Compounds. J. Electrochem. Soc., 151, A31-A39.

Lin, D., Tian, X., Wu, F., Xing, B. (2010). Fate and transport of engineered nanomaterials in the environment. J. Environ.l Qual., 39, 1896-1908.

Lovley, D. R., Stolz, J. F., Nord, G. L., Phillips, E. J. P. (1987) Anaerobic Production of Magnetite by a Dissimilatory Iron-Reducing Microorganism. Nature, 330, 252-254.

Mackenzie, K., Bleyl, S., Georgi, A., Kopinke, F.-D. (2012). Carbo-Iron – An Fe/AC composite – As alternative to nano-iron for groundwater treatment, Water Res. 46, 3817-3826.

Mackenzie, K., Bleyl, S., Kopinke, F.-D., Doose H., Bruns, J. (2016). Carbo-Iron as improvement of the nanoiron technology: From laboratory design to the field test, Sci. Tot. Environ. 563–564, 641-648.

Muhamadali, H., Xu, Y., Ellis, D. I., Allwood, J. W., Rattray, N. J. W., Correa, E., Alrabiah, H., Lloyd, J. R., Goodacre, R. (2015) Metabolic Profiling of Geobacter sulfurreducens during Industrial Bioprocess Scale-Up. Appl. Environ. Microbiol. 81, 3288-3298.

Murmann, R.-K., Robinson, P.-R. (1974) Experiments utilizing FeO_4^{2-} for purifying water. Water Res. 8, 543-547.

Petrovic, J., Thomas, G. (2010) A Study of Issues Related to the Use of Aluminum for On-Board Vehicular Hydrogen Storage. U.S. Department of Energy.

Phenrat, T., Fagerlund, F., Illangasekare, T., Lowry, G. V., Tilton, R. D. (2011). Polymer-modified Fe0 nanoparticles target entrapped NAPL in two dimensional porous media: effect of particle concentration, NAPL saturation, and injection strategy. Environ. Sci. Technol., 45, 6102-6109.

Phenrat, T., Saleh, N., Sirk, K., Kim, H. J., Tilton, R. D., Lowry, G. V. (2008). Stabilization of aqueous nanoscale zerovalent iron dispersions by anionic polyelectrolytes: adsorbed anionic polyelectrolyte layer properties and their effect on aggregation and sedimentation. J. Nanopart. Res., 10, 795-814.

Ryan, J. N., M. Elimelech (1996). A collection of papers presented at the Symposium on Colloidal and Interfacial Phenomena in Aquatic EnvironmentsColloid mobilization and transport in groundwater. Coll. Surfaces A: Physicochem. Engin. Aspects 107, 1-56.

Suresh, S. (2009) Reductive Remediation of Pollutants Using Metals. Open Waste Manag. 2, 6-16.

Tiwari D., Lee S.-M. (2011) Ferrate(VI) in the Treatment of Wastewaters: A New Generation Green Chemical, Waste Water - Treatment and Reutilization. ISBN: 978-953-307-249-4. InTech.

Tosco, T., Bosch, T., Meckenstock, R.U., Sethi, R. (2012) Transport of ferrihydrite nanoparticles in saturated porous media: role of ionic strength and flow rate. Environ. Sci. Technol. 46, 4008-4015.

US EPA – USA Environmental Protection Agency (2002) Report EPA-821-R-02-012, Methods for measuring the acute toxicity of effluents and receiving waters to freshwater and marine organisms. EPA-821-R-02-012.

Section 7.2.3.1

Watts, M. P.,Coker, V. S., Parry, S., Pattrick, R. A. D., Thomas, R. A. P., Kalin, R., Lllyod, J. R., (2015) Effective treatment of alkaline Cr(VI) contaminated leachate using a novel Pd-bionanocatalyst: Impact of electron donor and aqueous geochemistry. Appl. Catal. B: Environmental, 170-171, 162-172.

Watts, M. P.,Coker, V. S., Parry, S., Pattrick, R. A. D., Thomas, R. A. P., Kalin, R., Lllyod, J. R., (2014) Biogenic nano-magnetite and nano-zero valent iron treatment of alkaline Cr(VI) leachate and chromite ore processing residue. Appl. Geochem., 27-42.